Subtilases turn on pectin methylesterase activity for a robust apoplastic immunity

Daniele Coculo[1], Daniele Del Corpo[1], Miguel Ozáez Martínez[2], Pablo Vera[2], Gabriella Piro[3], Monica De Caroli[3] and Vincenzo Lionetti[1, 4]*.

* Address correspondence to Vincenzo Lionetti (vincenzo.lionetti@uniroma1.it)

Keywords: Pectin Methylesterases, Subtilases, Plant Immunity, *Botrytis cinerea*, *Arabidopsis thaliana*, Cell Wall Integrity

1 Dipartimento di Biologia e Biotecnologie Charles Darwin, Sapienza Università di Roma, Rome, Italy

2 Instituto de Biologia Molecular y Celular de Plantas, Universidad Politecnica de Valencia-C.S.I.C, Ciudad Politecnica de la Innovacion, Valencia, Spain.

3 Dipartimento di Scienze e Tecnologie Biologiche e Ambientali, Università del Salento, Lecce, 73100 Italy

4 CIABC, Sapienza Università di Roma, Rome, Italy

One sentence Summary: Subtilases arm pectin methylesterase activity against pathogens to switch on pectin integrity signalling, reinforcing plant immunity and avoiding the growth-defense trade-offs

Running title: Subtilases arm PME activity in plant immunity

Abstract

Plants involve a fine modulation of pectin methylesterase (PME) activity against microbes. PME activity can promote the cell wall stiffening and the production of damage signals able to induce defense responses. However, to date, the knowledge about the molecular mechanisms triggering PME activity during disease remains largely unknown. In this study, we explored the role of subtilases (SBTs), serine proteases consisting of 56 isoforms in *Arabidopsis thaliana,* as activators of PME activity in plant immunity. By using biochemical and reverse genetic approaches, we found that SBT3.3 and SBT3.5 are required to control PME activity and resistance to the fungus *Botrytis cinerea. Arabidopsis sbt3.3 and sbt3.5* knockout mutants showed a reduced induction of PME activity and an increased susceptibility to *B. cinerea*. *SBT3.3* expression is controlled by the damage-associated molecular patterns Oligogalacturonides. The *SBT3.3* overexpression overactivates PME activity, but only during fungal infection, resulting in an increased expression of the defense-related genes and in an enhanced resistance to *B. cinerea*. We revealed that SBT3.3 and the Pro-PME17 isoforms are both secreted in the cell wall exploiting distinct protein secretion pathways and a different kinetic. Our findings point to SBTs as a mechanism to switch on PME activity and the related pectin integrity signaling to strengthen plant immunity against pests, in a timely manner to avoid the growth-defense trade-off.

35 **Introduction**

36 Plants continuously perceive attacks by microorganisms activating a timely and effective immune
37 response. Part of this recognition is exerted by plasma membrane Pattern Recognition Receptors
38 (PRRs), which can detect Microbe-, Pathogen-, or endogenous Damage Associated Molecular Patterns
39 (MAMPs, PAMPs or DAMPs)(Zhou and Zhang, 2020). Pattern-triggered immunity (PTI) constitutes
40 the first line of plant inducible immunity that restricts pathogen proliferation. Since the immunity
41 efforts often result in a growth defense trade-offs, a precise regulation of immune pathways becomes
42 critical to optimize fitness (Lionetti et al., 2010; Huot et al., 2014; Ha et al., 2021). A pivotal role in
43 this homeostasis is played by proteolysis mediated by proteases, widely implicated in plant stresses,
44 although their action mechanisms remain largely unknown (Schaller, 2004; Hou et al., 2018). In
45 particular, Subtilases (SBTs, Pfam00082), serine peptidases belong to family S8, (MEROPS database;
46 https://www.ebi.ac.uk/merops/cgi-bin/famsum?family=S8) plays key roles in defense responses against
47 microbes, plant parasitism and adaptation to the environmental changes (Figueiredo et al., 2018;
48 Schaller et al., 2018; Ogawa et al., 2021). In *A. thaliana,* 56 SBT isoforms are divided into 6
49 subfamilies: SBT1, SBT2, SBT3, SBT4, SBT5, SBT6 (Rautengarten et al., 2005).

50 Specific SBTs are targeted to the plant Cell Wall (CW), the foremost interface at which interactions
51 between plants and microbes take place, to trigger specific protease-activated defense signaling
52 (Doehlemann and Hemetsberger, 2013). In this compartment, SBTs can process larger precursor
53 zymogens (Pro-Proteins), that require specific activation processes for enzyme maturation (Khan and
54 James, 1998). SBT6.1 (S1P) can process the pro-peptide form of RAPID ALKALINIZATION
55 FACTOR 23 (RALF23) modulating immune response against *Pseudomonas syringae* (Stegmann et al.,
56 2017). In tomato, specific SBTs contributes to Jasmonic Acid-mediated resistance against *Manduca*
57 *sexta* larvae, by processing the wound pro-hormone Prosystemin, releasing the bioactive peptide called
58 Systemin (Meyer et al., 2016). The six genes of the tomato cluster SBT P69 (P69A–P69F) express
59 proteins particularly involved in plant defense. P69B can cleave the *Phytophthora infestans* PC2, a
60 cysteine-rich secreted apoplastic protein releasing immunogenic peptides that activates host immunity
61 (Wang et al., 2021). In particular, P69C processes an extracellular matrix-associated Leucine-Rich
62 Repeat protein (LRP), the first physiological target of an extracellular SBT identified in plants (Tornero
63 et al., 1996). SBT3.3, the ortholog of tomato P69C in *Arabidopsis*, was discovered as regulator of
64 *Arabidopsis* primed immunity (Ramirez et al., 2013). Although SBT3.3 was postulated to cleave an

65 extracellular larger protein, the identification of its specific substrate and the mechanism by which
66 SBT3.3 can trigger immunity remains to be identified.

67 During plant development, specific SBTs can process specific Pectin Methylesterases (PME;
68 Pfam01095), enzymes regulating the methylesterification of Homogalacturonan (HG), the major
69 constituent of pectin in the CW (Wormit and Usadel, 2018; Coculo and Lionetti, 2022). PMEs catalyse
70 the hydrolysis of methylester bonds at C-6 of Galacturonic Acid (Gal A) residues, producing acidic
71 pectins with negatively charged carboxyl groups, releasing methanol (MeOH) and protons into the
72 apoplast. In *Arabidopsis*, 66 PME isoforms have been identified which can be classified into 2 groups
73 on the basis of their structures (Pelloux et al., 2007; Dedeurwaerder et al., 2008). Group 1 comprises 21
74 PME isoforms, containing only the catalytic domain. The 45 PME isoforms of Group 2 (hereafter
75 named Pro-PMEs) are organized as a polycistronic messenger RNA which resembles an operon-like
76 gene cluster (Coculo and Lionetti, 2022). In Pro-PMEs, the PME catalytic domain is preceded by an
77 N-terminal region (also referred as Pro region or PMEI-like domain) which shares structural
78 similarities with functionally characterized PME Inhibitors (PMEIs) and that can acts as auto-inhibitor
79 of PME activity (Bosch et al., 2005; Wolf et al., 2009; Del Corpo et al., 2020). This domain could
80 impede a premature pectin de-methylesterification, during specific phases of their secretion, assembly,
81 or modification contributing to a correct pectin functionality.

82 A local and strong induction of PME activity is exerted in *Arabidopsis thaliana* and other plants, when
83 challenged with different microbial pathogens (Bethke et al., 2014; Lionetti, 2015; Lionetti et al.,
84 2017). *Pro-PME17* isoform is strongly upregulated in response to several pathogens, defense
85 hormones, elicitors or abiotic stress and its activity strongly contribute to the induction of defense-
86 related PME activity (Bethke et al., 2014; Del Corpo et al., 2020). A finely tuned PME activity can
87 play multiple functions in plant immunity. PMEs can produces de-methylesterified negatively charged
88 carboxyl groups that can form consecutive calcium bonds with other HG molecules and thus
89 strengthen the CW through the formation of "egg-boxes" structures (Senechal et al., 2014b; Del Corpo
90 et al., 2020). Plant PME activity can also favour DAMP related immunity. In particular, the PME
91 activity could favour the release and perception of de-methylesterified oligogalacturonides (OGs), the
92 well characterized DAMP, locally released in cooperation with endo-polygalacturonases (PGs), and
93 able to trigger plant immunity (Osorio et al., 2008; Osorio et al., 2011; Ferrari et al., 2013; Kohorn et
94 al., 2014). OGs are perceived in *Arabidopsis* by the pathogen recognition receptor WALL-
95 ASSOCIATED KINASE1 (WAK1) to activate plant immune responses (Brutus et al., 2010; Kohorn

96 and Kohorn, 2012). WAK2 requires PME-mediated pectin de-methylesterification to activate OGs-
97 dependent stress responses (Kohorn et al., 2014). Interestingly, WAK1, WAK2 and another PRR,
98 FERONIA (FER), preferentially bind to de-methylesterified pectins (Decreux and Messiaen, 2005;
99 Kohorn et al., 2014; Feng et al., 2018; Guo et al., 2018; Lin et al., 2021). The de-methylesterification of
100 pectin by PMEs represents the main mechanism to generate plant-derived methanol (MeOH), a DAMP-
101 like alarm signal (Hann et al., 2014). OGs and MeOH are able to trigger defensive priming effect
102 setting the stage for the intra and inter-plant immunity (Dorokhov et al., 2012; Komarova et al., 2014;
103 Gamir et al., 2021; Giovannoni et al., 2021).

104 Precise switch on/off mechanisms regulating plant immunity are required because they must be timely
105 triggered for an efficient immune response and they cannot be persistent given the well-known defense
106 growth trade-off (He et al., 2022). The need of a post-transcriptional control of PME activity by
107 specific PME inhibitors (PMEIs) late during plant invasion by microbes was previously demonstrated
108 (An et al., 2008; Lionetti et al., 2017; Liu et al., 2018). The involvement of SBTs as posttranscriptional
109 processing of Pro-PMEs and regulation of PME activity in plant immunity was still not investigated.
110 Here, we found that all the PME isoforms induced in *A. thaliana* against the necrotrophic fungus
111 *Botrytis cinerea* possess a Pro-region. Exploiting reverse genetic approaches and biochemistry, we
112 demonstrated that SBT3.3 and SBT3.5 contribute to the induction of PME activity in *Arabidopsis*
113 immunity against *Botrytis*. Notably, we found that SBT3.3 processes defense related Pro-PMEs as
114 substrate and trigger specific defense related genes. SBT3.3 and Pro-PME17 follows distinct secretion
115 pathways to reach the apoplast where they later colocalize. Our results provide strong evidence that the
116 processing of Pro-PMEs by SBTs represents a mechanism to switch on PME activity and the related
117 pectin integrity signaling for a timely immune response, avoiding the growth-defense trade-offs.

118 **RESULTS**

119 **The processing of Pro-PME zymogens is required in *Arabidopsis-Botrytis* interaction**

120 *PMEPCRA*, *PME3, PME17*, *PME20*, *PME21*, and *PME41* are the PME isoforms exhibiting a
121 significant altered timing and level of expression in *A. thaliana* - *B. cinerea* interaction and in several
122 other pathosystems (Lionetti et al., 2012; Bethke et al., 2014; Lionetti et al., 2017). Interestingly, after a
123 careful comparison of the sequences we realized that all these isoforms are zymogens, expressed as
124 Pro-PME inactive precursors (Supplemental Figure S1). This strongly suggests that a proteolytic
125 cleavage, exerted by specific proteases, is requested for PME activation in *Arabidopsis* immunity

126 against *Botrytis*. While the PME catalytic domain is highly conserved, we intriguingly noticed here a
127 variability in the processing motif between the different PME isoforms. Pro-PMEPCRA, Pro-PME17
128 and Pro-PME21 showed a RKLL processing motif, while the RRKL motif characterized the Pro-
129 PME20 and Pro-PME41 isoforms. Instead, two processing motifs, RKLK and RRLL were present in
130 the Pro-PME3. Other motifs with the consensus sequence FPSW and LPLKMTERARAV are partially
131 conserved between the isoforms. All these observations could imply the involvement of multiple
132 proteases-PME pairs.
133

134 **_SBT3.3_ and _SBT3.5_ are induced in _Arabidopsis_ during _B. cinerea_ as part of PTI**

135 We explored the possibility that SBTs are involved in the processing and activation of Pro-PMEs
136 against microbes. Exploiting publicly available microarray data, we selected two genes, *SBT3.3* and
137 *SBT3.5* showing a significative induction during *B. cinerea* infection (Supplemental Figure S2A).
138 Interestingly, both genes are co-expressed with *Pro-PME17,* a functional PME involved in the
139 resistance to *Botrytis cinerea* (Supplemental Figure S2B) (Lionetti et al., 2012; Del Corpo et al., 2020).
140 To confirm the transcriptomic analysis and to gain more insight in the kinetic of expression of these
141 genes during the disease, the expression levels of *SBT3.3* and *SBT3.5* were quantified at different times
142 in *B. cinerea*-infected and Mock-inoculated *A. thaliana* wild type (WT) leaves by qPCR (Figure 1A
143 and B). *SBT3.3* is expressed only in infected tissues while *SBT3.5* shows a basal expression also in
144 Mock-inoculated leaves. *SBT3.3* and *SBT3.5* were significantly induced at 24 hpi and further increased
145 at 48 hpi, when they showed about a significant 15- and 5-fold induction, respectively, in infected
146 leaves compared to Mock inoculated tissues. These data clearly reveal an involvement of *SBT3.3* and
147 *SBT3.5* in *Arabidopsis-Botrytis* interaction. Interestingly, the expression of both *SBTs* is also triggered
148 in *Arabidopsis* against several pathogens and by different bacterial and fungal elicitors of plant defense
149 responses (Supplemental Figure S3). We next investigated whether pectin-related DAMPs can impact
150 on the expression of the selected SBTs. *Arabidopsis* WT seedlings were treated with OGs or water, and
151 the expression of *SBT3.3* and *SBT3.5* was evaluated at 1 h post treatment. A 7-fold induction of *SBT3.3*
152 was revealed after treatment with OGs (Supplemental Figure S3 and Figure 1C), while the expression
153 of *SBT3.5* was not induced (Supplemental Figure S3 and Figure 1D). All these results indicate that
154 *SBT3.3* and *SBT3.5* are part of *Arabidopsis* immune responses against *B. cinerea* and several
155 pathogens.

156

157 **SBT3.3 and SBT3.5 contribute to *Arabidopsis* PME activation and resistance to *B. cinerea***

158 To explore on the possibility that SBT3.3 and SBT3.5 may be involved in the activation of Pro-PMEs
159 in plant immunity we exploited a reverse genetic approach. Two T-DNA insertional mutants for the
160 selected genes were isolated (Figure 2A). The insertions were localized in the fifth and ninth exons,
161 respectively, for *sbt3.3-1* (SALK_086092) and *sbt3.3-2* (SALK_107470.45.45) mutants and in the first
162 exon and in the second intron, respectively for *sbt3.5-1* (SAIL_400_F09) and *sbt3.5-2* (GABI_672C08)
163 mutants. The level of *SBT3.3* and *SBT3.5* expression was compared in leaves of mutants and WT plants
164 after *B. cinerea* and Mock inoculation by qPCR (Figure 2B). All mutants fail to induce gene expression
165 in fungus-challenged leaves, resulting in *sbt3.3* and *sbt3.5* KO lines. No significant defects were
166 observed in the rosette growth and seed germination in *sbts* mutants which showed growth parameters
167 similar to WT plants (Figure 2C and S4A and B). To understand if the lack of *SBTs* expression can
168 influence pectin composition we compared the monosaccharide composition of matrix polysaccharides
169 extracted from rosette leaves of *sbts* mutants and WT plants. All mutants analysed showed a molar
170 percentage of monosaccharides not significantly different from that observed in WT plants (Figure 2D).
171 After establishing that the two SBTs are involved in *Arabidopsis-Botrytis* interaction we evaluated their
172 possible contribution in the control of PME activity during fungal infection. The level of PME activity
173 was quantified in leaves of WT, *sbt3.3-1*, *sbt3.3-2, sbt3.5-1* and *sbt3.5-2* plants at 24 hours post
174 *Botrytis* and Mock inoculation using histochemical and biochemical assays based on Ruthenium Red
175 (RR), a cationic dye with six positive charges able to bonds with the acidic groups of HG (Lionetti,
176 2015)(Figure 3A). A significant lower induction of PME activity was observed in infected *sbt3.3-1*,
177 *sbt3.3-2*, *sbt3.5-1* and *sbt3.5-2* mutants (respectively of 3.7-, 3.1, 1.9- and 1.8-fold reduction) compared
178 to WT (Figure 3B). These results unveil for the first time that Pro-PMEs are substrates for SBT3.3 and
179 indicate that SBT3.3 and SBT3.5 contribute to control the PME activity in *Arabidopsis* immunity to
180 *Botrytis.* Interestingly, the significant difference found in *sbt3.3* respect to *sbt3.5* mutants suggest that
181 the two proteases can process different Pro-PMEs isoforms during disease. No significant differences
182 in PME activity were observed between Mock-inoculated WT plants and *sbt* mutants. This was
183 expected for *sbt3.3* mutants, as *SBT3.3* is not basally expressed in leaves (Figure 1A). In *sbt3.5*
184 mutants, the lack of the basal *SBT3.5* expression in *Mock*-inoculated leaves (Figure 2B) does not
185 significantly affect the monosaccharide composition and the total PME activity in leaves (Figure 2D
186 and 3B) as well as on the rosette growth and seed germination (Figure 2C and Supplemental Figure
187 S4). Therefore, we evaluated the susceptibility of *sbt3.3* and *sbt3.5* mutants to *B. cinerea* (Figure 4A
188 and B). The local symptoms of the fungus were significantly higher in both *sbt3.3* and *sbt3.5* mutants

189 respect to WT. In particular, the lesion areas produced by the fungus were larger in *sbt3.3-1*, *sbt3.3-2,*
190 *sbt3.5-1*, *sbt3.5-2* mutants (respectively, of 2.2-, 2.1, 1.7- and 1.7-folds) respect to WT. A greater
191 development of *Botrytis* mycelium was detected in *sbt* mutants respect to WT plants using trypan blue
192 staining (Figure 4B). All our results indicate that, although at different extent, both SBTs contribute to
193 trigger PME activity and the resistance to *Botrytis*. A correlation between the level of resistance and the
194 amount of PME activity expressed in the tissues were observed between the different genotypes
195 analysed (Figure 3 and 4).
196
197 **SBT3.3 overexpression overactivates defense related PME activity restricting *Botrytis* infection**
198 Given the lower induction of PME activity observed in *sbt3.3* mutants compared to those of SBT3.5,
199 we deepen our study on SBT3.3 exploring the effect of its overexpression in *Arabidopsis* on PME
200 activity and *Botrytis* resistance. Two transgenic *Arabidopsis* lines, named *SBT3.3-OE1* and *SBT3.3-*
201 *OE2* exhibiting high level of SBT3.3 expression in leaves were characterized (Figure 5A).
202 Interestingly, an 85- and 90-fold overexpression was revealed, respectively, in leaves of *SBT3.3-OE1*
203 and *SBT3.3-OE2* lines respect to WT leaves when infected with *B. cinerea*. No growth abnormalities
204 were observed in *SBT3.3* overexpressing plants (Figure 5B and S4). The CW monosaccharide
205 composition in rosette leaves of SBT3.3-OE lines is not significantly different from that quantified in
206 the WT plants (Figure 5C). These results are consistent with those obtained with the mutants and
207 corroborate the conclusion that the expression of *SBT3.3* is dedicated to the *Arabidopsis* immune
208 response. The level of PME activity was quantified in leaves of WT, *SBT3.3OE-1 and SBT3.3OE-2*
209 plants at 24h post *Botrytis*- and Mock-inoculation (Figure 6A). A significant higher induction of
210 defense-related PME activity was observed in the infected *SBT3.3* overexpressing lines compared to
211 control. *SBT3.3OE-1* and *SBT3.3OE-2* lines showed, respectively, a 3.1- and 2.3- fold increase of PME
212 activity in the *B. cinerea* infected leaves compared to WT. Despite the *SBT3.3* overexpression in
213 transgenic Mock-inoculated plants, the level of PME activity were not significantly different from that
214 measured in WT plants (Figure 6A). This result highlights that SBT3.3 triggers PME activity
215 exclusively in *Arabidopsis* defense against the fungus. The levels of methylesters remained in the CW
216 after 24 h of *B. cinerea* inoculation were compared between *SBT3.3-OE* lines and WT plants. A
217 significant lower amount of methylesters was revealed in the CW extracted from *B. cinerea* infected
218 leaves of *SBT3-3-OE1* and *SBT3.3-OE2* lines respect the WT plants (Figure 6B). This result confirms
219 that SBT3.3 processes the Pro-PMEs in plant defense and that a higher PME activity was released by
220 SBT3.3 overexpression in transgenic plants challenged with the fungus respect the control.

221 Next, we evaluated the susceptibility of *SBT3.3-OE* lines to *B. cinerea*. The local symptoms of the
222 fungus were significantly lower in both *SBT3.3-OE* plants when compared with the WT (Figure 6C and
223 D). In particular, the lesion area produced by the fungus in *SBT3.3-OE1* and *SBT3.3-OE2* mutants are
224 2- and 1.5-fold lower compared to WT. A minor development of *Botrytis* mycelium was detected in
225 *SBT3.3-OE1* plants respect to WT plants using trypan blue staining (Figure 6D). All these results
226 support an important role of SBT3.3 as trigger of PME activity in *Arabidopsis* immunity to *Botrytis*
227 and indicate that the SBT3.3 overexpression confers to *Arabidopsis* a higher resistance to *B. cinerea*
228 respect to WT.
229
230 ***SBT3.3* overexpression enhances immune responses against *Botrytis***
231 The next goal was to verify whether the improved resistance observed in the SBT3.3 overexpressing
232 lines could be linked to a more robust immune response. The induction of an array of defense related
233 genes important for *Arabidopsis* defense against *Botrytis* was compared between WT and *SBT3.3-OE1*
234 plants inoculated with Mock and *Botrytis*. *WRKY33* is a key transcriptional regulator of hormonal and
235 metabolic responses toward *B. cinerea* infection (Birkenbihl et al., 2012). *WRKY33* can targets the
236 promoter of *PHYTOALEXIN DEFICIENT3 (PAD3)* encoding an enzyme required for the synthesis of
237 antimicrobial camalexin (Zhou et al., 1999). The cytochrome P450 enzyme *CYP81F2* is essential for
238 the pathogen-induced accumulation of 4-methoxy-indol-3-ylmethyl Glucosinolate (Clay et al., 2009;
239 AbuQamar et al., 2017). *WAK2* is a wall associated kinase mediating pectin related immunity and
240 activated by de-methyl esterified pectin to trigger defense responses (Kohorn et al., 2014). *PME17* and
241 *PMEI10* are two regulators of PME activity in plant immunity to *B.cinerea* (Lionetti et al., 2017; Del
242 Corpo et al., 2020). Interestingly, a higher induction of *WRKY33*, *PAD3*, and *WAK2* were observed in
243 *SBT3.3-OE1* plants respect the WT only when challenged with the fungus (Figure 7). *CYP81F2*
244 showed levels of expression similar between WT and *SBT3.3-OE1* plants. However, considering the
245 lower level of *B. cinerea β-tubulin* and the lower fungal symptoms observed in transgenic plants
246 (Figure 7 and Figure 6C and D) it is possible to conclude that also CYP81F2 expression is stimulated
247 by *SBT3.3* overxpression. The *Pro-PME17* and *PMEI10* expressions seems independent from SBT3.3
248 activity since their inductions follow the extent of fungal infection and *B. cinerea β-tubulin* expression.
249 These findings indicate that SBT3.3 contribute to enhance *Arabidopsis* immunity, most likely,
250 improving the production of antimicrobial compounds and reinforcing cell wall integrity surveillance.
251 We next explored if SBTs expression can influence Hydrogen Peroxide production, an important
252 defense response to *Botrytis* infestation (Pogorelko et al., 2013; Siegmund and Viefhues, 2016). Leaves

253 of WT, *sbt3.3-1*, *sbt3.5-1* and *SBT3.3-OE1* plants, were inoculated with Mock or *B. cinerea* and stained
254 with 3,3′-diaminobenzidine, a chromogen able to reveal the H_2O_2 accumulation in the tissue (Reem et
255 al., 2016). No accumulation of H_2O_2 was observed in Mock-inoculated leaves of all genotypes
256 analyzed and a similar DAB staining was revealed in all the leaves challenged with *Botrytis*. These
257 results indicate that H_2O_2 production is not dependent from SBTs mediated signaling (Supplemental
258 Figure S5).
259

260 **SBT3.3 and Pro-PME17 are secreted through distinct protein secretion pathways in the apoplast**
261 **where lastly colocalized**

262 SBT3.3 was previously found in the extracellular compartment, but its secretion pathway was never
263 explored (Ramirez et al., 2013). Moreover, Pro-PME17 was predicted to be an apoplastic protein, but
264 its localization was never demonstrated. With the aim to deepen our knowledge on the secretion
265 patterns and the final subcellular destination of the two proteins, a fluorescent variant of SBT3.3 and of
266 Pro-PME17 were constructed by fusing the respective encoding cDNA to *yfp* and *gfp,* under the control
267 of *35S* promoters. The fluorescent tag was linked to the C-terminus of both proteins, as none of them
268 are predicted to have the ω site of the glycosylphosphatidylinositol (GPI) anchor addition (predGPI
269 software; http://gpcr2.biocomp.unibo.it/predgpi/), as previously found for AtPMEI1 (De Caroli et al.,
270 2011). *SBT3.3-YFP* and *Pro-PME17-GFP* constructs were transiently expressed in the epidermal cells
271 of tobacco leaves and observed by laser scanning confocal microscopy (Figure 8). Both proteins
272 accumulate in the apoplast as confirmed by colocalization with the CW marker XTH11-RFP (De Caroli
273 et al., 2021) (Figure 8A-C, Q-S) and plasmolysis of epidermal cells co-expressing both *pm-rk*, marker
274 of plasma membrane (Nelson et al., 2007) and *SBT3.3-YFP* or *Pro-PME17-GFP* (Figure 8D, T).
275 Nevertheless, the fluorescence signals relative to SBT3.3-YFP and Pro-PME17-GFP showed different
276 secretion patterns. SBT3.3-YFP exhibited a typical cytosolic fluorescent pattern, labelling the
277 nucleoplasm and appearing excluded by the ER and Golgi stacks, without any colocalization with the
278 specific organelle markers, RFP-HDEL and ST52-mCherry, respectively (Nelson et al., 2007) (Figure
279 8A-J). Other than nucleoplasm and cell wall, SBT3.3-YFP labelled small cytosolic punctate structures
280 that significantly colocalized with the Exocyst Positive Organelles (EXPOs) marker Exo70E2-GFP
281 (Wang et al., 2010; Wang et al., 2017) indicating the possible involvement of EXPOs in an
282 unconventional trafficking of the chimera toward the CW (Figure 8K-M). Proteins that follow the
283 Unconventional Secretion Pathway (UPS) bypass the Golgi and are insensitive to brefeldin A (BFA),

284 an inhibitor of ER-Golgi trafficking (Zhang et al., 2011). BFA treatment did not affect SBT3.3-YFP
285 secretion pattern while clearly perturbed the Golgi organization labelled by ST52-mCherry (Figure 8N-
286 P). A conventional secretion pathway is followed by Pro-PME17-GFP that labelled the ER, continuous
287 to the nuclear envelope, and small punctate structures colocalizing with the ER and the Golgi markers,
288 respectively (Figure 8U-Z). Intriguingly, the Pro-PME17 reaches the apoplast before the SBT3.3. At
289 48 h post transformation, the CW was intensely labelled by Pro-PME17-GFP and, at approximately 60
290 h by SBT3.3-YFP protein fusion (Figure 8A and Q). These results indicate that both SBT3.3 and Pro-
291 PME17 are correctly secreted into the apoplast by using different secretion pathways and in a
292 temporally staggered manner. We further explored the timing of SBT3.3 and Pro-PME17
293 colocalization into the cell wall using a new version of *Pro-PME17* tagged with *rfp,* under the control
294 of *35S* promoter transiently co-expressed with *SBT3.3-YFP* in the epidermal cells of tobacco leaves.
295 We confirmed that the the Pro-PME17 and SBT3.3 colocalize at the CW, and this is favoured over time
296 as revealed by colocalization parameters (Figure 9). All these results strongly support the hypothesis
297 that Pro-PME17 is secreted in an unprocessed and inactive form in the CW where, later when required,
298 is activated by SBT3.3 to trigger immunity.

299 **DISCUSSION**

300 Plants exploit a great and local increase of PME activity in response to pathogens with different
301 lifestyles (Bethke et al., 2014; Lionetti et al., 2014; Lionetti, 2015; Lionetti et al., 2017). *A. thaliana*
302 induces the expression of specific PME isoforms during the attack of different pathogens. Among
303 them, *Pro-PME17* is induced after the infection of a wide range of plant pathogens and can be
304 considered a general biomarker of pathogenesis (Lionetti et al., 2012). *Botrytis cinerea* is an important
305 fungal plant necrotrophic pathogen, that kills plant tissue prior to feeding using a range of toxic
306 molecules to destroy host cells (Williamson et al., 2007; Dean et al., 2012). Pro-PME17 was recently
307 involved in triggering PME activity and in resistance against *B. cinerea* (Del Corpo et al., 2020). The
308 Pro region acts as an intramolecular inhibitor of Pro-PME17 activity. Here, intriguingly we note that all
309 the PME isoforms induced in *A. thaliana* during *B. cinerea* infection are organized as zymogens in
310 which the catalytic region is preceded by an N-terminal Pro region. The structural similarity revealed
311 between the amino acid sequences of the Pro regions of these PMEs and the independent immunity-
312 related PMEIs (AtPMEI10 and AtPMEI11) (Lionetti et al., 2017; Del Corpo et al., 2020) support their
313 possible role as intramolecular inhibitors of the specific PMEs in each specific Pro-PME cluster. We
314 therefore attempted to identify which possible proteases could be involved in the activation of PME

315 activity against microbes. Different SBTs were associated to the processing of PMEs in plant
316 physiology (Schaller et al., 2018). Most SBTs are targeted to the CW, where they contribute to the
317 control of CW properties during growth and development. The *Arabidopsis* SBT3.5 was previously
318 found to process Pro-PME17 releasing PME activity during root growth in *Arabidopsis* seedlings
319 (Senechal et al., 2014a). SBT1.7 modulates PME activity in the mucilage release from *Arabidopsis*
320 seed coats (Rautengarten et al., 2008). AtSBT6.1 is likely to be involved in maturation of a pectin
321 methylesterase (Wolf et al., 2009). The evidence that the precursors of bZIP transcription factors,
322 RALF23 and GOLVEN1 are further substrates of AtSBT6.1 and that most SBTs are synthesized as
323 inactive precursors could suggest that SBTs isoform could be part of an activation cascade, similar to
324 that observed for caspases during plant programmed cell death events in mammals (Vartapetian et al.,
325 2011; Reichardt et al., 2018; Paulus and Van der Hoorn, 2019).

326 Although SBTs were also associated to plant immunity their molecular substrates and their function
327 remains largely unknowns (Figueiredo et al., 2014; Schaller et al., 2018; Godson and van der Hoorn,
328 2021). The tomato subtilisin-like protease SlSBT3 contributes to insect resistance in tomato. Although
329 SlSBT3 was found to affect PME activity and the level of pectin methylesterification, these effects
330 were unrelated to its role in herbivore defense (Meyer et al., 2016). Also, AtSBT5.2 and AtSBT3.14
331 were involved in different plant-pathogen interactions but their functions appear unrelated to PME
332 activity (Lozano-Torres et al., 2014; Serrano et al., 2016). Here, we explored on the possible role of
333 SBTs as post-transcriptional regulators of PME activity in *Arabidopsis* immunity against the
334 necrotrophic fungus *B. cinerea*. Exploiting publicly available microarray data, we selected two genes,
335 *SBT3.3* and *SBT3.5* co-expressed with *Pro-PME17* in *Arabidopsis* during *Botrytis* infection. SBT3.3
336 was previously discovered as a extracellular subtilase involved in the activation of *Arabidopsis*
337 immunity against *Pseudomonas syringae* and *Hyaloperonospora arabidopsidis* (Ramirez et al., 2013)
338 although its substrate remained unknown. Here, we demonstrated that *SBT3.3* and *SBT3.5* are induced
339 in *Arabidopsis* leaves challenged with *Botrytis*. *SBT3.3* exhibited a higher fold-induction respect to
340 SBT3.5. Interestingly, the expression of both *SBT* genes is also triggered in *Arabidopsis* against several
341 pathogens. Moreover, *SBT3.3* and *SBT3.5* are induced by different bacterial and fungal elicitors of
342 plant defense responses. SBT3.3 is specifically dedicated to plant defense because it is induced only
343 during the infection process. However previous evidence indicates that SBT3.3 expression respond
344 very rapidly to H_2O_2 and it enhances the activation of mitogen-activated protein kinases (MAPKs)
345 following microbial attack (Ramirez et al., 2013). We detected SBT3.3 as a component of OGs

346 signaling. All these evidence points to the involvement of SBT3.5 and, particularly of SBT3.3, as
347 contributors in the activation of the earliest signaling events of PTI against *Botrytis* and several other
348 pathogens.

349 The possible role of SBT3.3 and SBT3.5 as PME activators in *Arabidopsis* immunity against *B.*
350 *cinerea* infection was explored. *sbt3.3-1*, *sbt3.3-2, sbt3.5-1*, *sbt3.5-2* mutants showed a significant
351 higher susceptibility to the fungus when compared with WT. The significant lower induction of PME
352 activity observed in *B. cinerea*-infected *sbt3.3* and *sbt3.5* mutants respect to WT plants indicates that
353 SBT3.3 and SBT3.5 are involved in the release of mature active PMEs to contrast the microbial
354 invasion. The susceptibility- and PME-related effects are more marked in the *sbt3.3* mutant respect to
355 *sbt3.5* mutants suggesting that SBT3.3 can have a major contribution on the total PME activity
356 expressed in *Arabidopsis* against the fungus. This also suggests that the two SBTs analyzed in this
357 study can target different Pro-PME isoforms. The involvement of multiple SBT-Pro-PME pairs is also
358 suggested by the observed variability in the processing motifs of all the PME isoforms involved in
359 *Arabidopsis-Botrytis* interaction. We revealed a significant higher induction of PME activity and a
360 higher resistance to *Botrytis* in infected *SBT3.3-OE1* and *SBT3.3-OE2* leaves respect to untransformed
361 plants. Overall, our evidence indicates that SBT3.3 and SBT3.5, by processing different Pro-PME
362 isoforms, contribute to trigger PME activity to contrast *B. cinerea* infection. The absence of growth
363 abnormalities and alteration of monosaccharide composition in the *sbt* mutants and SBT3.3OE lines
364 indicate that these SBTs are mostly involved in plant immunity processes in leaves of adult plants.
365 The low level of CW methylesters detected in SBT3.3OE lines indicate that SBTs, by timely activating
366 PMEs early at the point of fungal penetration, can favor the increase of charged carboxyl groups
367 forming a higher amount of Ca^{2+}-mediated pectin crosslinks to reinforce the CW structure and the
368 resistance to the microbe. Moreover, the SBT3.3-related pectin structural reinforcement is also
369 accompanied by the stimulation of an immune response signaling. The higher induction of *WRKY33*,
370 *PAD3*, *CYP81F2* and *WAK2* genes detected in *SBT3.3-OE1* plants respect to WT plants identifies a
371 more robust immune response as mechanism contributing to the improved resistance observed in the
372 transgenic plants. The induction of *WRKY33*, *PAD3* and *CYP81F2* by *SBT3.3* overexpression suggests
373 the involvement of Camalexin and indole Glucosinolate accumulation. The evidence that WAK2 is
374 highly expressed in transgenic plants suggest also the improvement of cell wall surveillance (Kohorn et
375 al., 2014). Interestingly, WAK2 was demonstrated to require PME-mediated pectin de-
376 methylesterification to activate OGs-dependent stress responses. We can hypothesize that SBT3.3

377 activates PME activity to favour WAK2 binding, and WAK2-OGs mediated stress signalling.
378 Considering that OGs induce the expression of *SBT3.3*, *WRKY33*, *PAD3* and *CYP81F2* and that a
379 *SBT3.3* self-activation was previously reported (Denoux et al., 2008; Ramirez et al., 2013), a positive
380 feedback loop circuit based on PME activity, could be mounted to strengthen the activation of OGs-
381 mediated defense responses. In addition, SBTs-dependent PME activity could also favour the binding
382 and the functions of other PRR, like WAK1 and FERONIA, known to preferentially bind de-
383 methylesterified crosslinked pectins (Decreux and Messiaen, 2005; Feng et al., 2018; Guo et al., 2018;
384 Lin et al., 2018). Future efforts will be needed to explore on these hypotheses. All these observations
385 indicate SBTs and PME activities exploit a cooperation between CW integrity maintenance and PTI
386 signalling to regulate defense responses after a CW damage (Engelsdorf et al., 2018).
387 Although the specific pairs of SBT3.3, SBT3.5 and Pro-PMEs involved in plant immunity remain to be
388 identified, we found that Pro-PME17 and SBT3.3 are both delivered in the apoplast although with
389 different secretion pathways. While Pro-PME17 follows a conventional secretion pathway, SBT3.3
390 undergoes an unconventional route since bypass the Golgi, is BFA insensitive and colocalizes with
391 Exo70E2, a subunit of the exocyst complex specifically identified in the EXPOs involved in
392 unconventional exocytosis. To date, SAMS2, involved in lignin methylation and XTH29, an
393 endotransglucosylase/hydrolases, are the two cell wall proteins reported to be secreted as EXPO cargo
394 ((Wang et al., 2010; De Caroli et al., 2021). As previously proposed, EXPOs-mediate secretion
395 emerges as a toolkit exploited by plants to ensure a dynamic remodelling of the cell wall structure able
396 to adapt to changing environmental and growing conditions (de la Canal and Pinedo, 2018). Moreover,
397 Pro-PME17 reaches the CW before SBT3.3 and their colocalization in the apoplast increase over time.
398 These spatio-temporal separations could avoid a premature PME activation and pectin de-
399 methylesterification during the secretion int the CW. Plants can accumulate Pro-PMEs clusters as
400 soluble and inactive receptors in the apoplast. At the right time, SBTs could be delivered in an apoplast
401 already enriched in the inactive Pro-PMEs, to unblock the inhibitory activity exerted by the Pro region
402 in a compartment-specific manner, rapidly derepressing PME activity. This mechanism could lead to a
403 faster induction of PME activity at the point of pathogen penetration to amplify the early immune
404 signalling underlying the defense response. The speed of a response, particularly to biotic stress, can be
405 crucial for the survival of the sessile plant. In a similar mechanism, known as ectodomain shedding, the
406 proteolytic cleavage of extracellular domains of cell surface proteins resulting in the activation of a
407 variety of normal and pathological signalling processes in animals including growth factor signalling,
408 cell adhesion, inflammation and cell survival (Lichtenthaler et al., 2018). This proposed SBTs function

409 would be also in line with the de-repression that speeds the responsiveness of hormonal transcription
410 networks in plants (Rosenfeld et al., 2002). It is important to remember that also SBTs are Pro-
411 peptides, in which the PRO region serves both as intramolecular chaperones required for enzyme
412 folding and as inhibitor of the mature proteases (Hohl et al., 2017). All this evidence suggests the
413 existence of mechanisms that accumulate multiple inactive molecular tools at the cell surface to be
414 turned on at the right time to amplify a cell wall integrity signalling leading to cell solution to contrast
415 pests. Many efforts are still required for the identification of the factors underlying these mechanisms
416 although the pH variation in the apoplast also important during microbe invasion seems to be involved
417 (Janzik et al., 2000; Geilfus, 2017).
418 Interestingly, SBT3.3 was involved in the physiological state called "priming", a sensory status able to
419 induce a resistance faster and stronger respect to the same stimulus received before (Ramirez et al.,
420 2013). SBT3.3 expression mediates the activation of chromatin remodelling of defence genes including
421 a self-activation, suggesting a positive feedback loop circuit to potentiate the defence response and
422 keep cells in a sustained sensitised mode. Our observation on the localization of SBT3.3-YFP in the
423 nucleus is consistent with this proposed role for this SBT. It was previously hypothesized that
424 "priming" could involve the accumulation of inactive proteins that becomes operative to initiate a
425 signal amplification leading to a faster and stronger activation of defense responses (Bruce et al., 2007;
426 Conrath, 2011; Ramirez et al., 2013). The processing of Pro-PMEs by SBT3.3, timely accumulated,
427 thanks to a spatial and temporal separation in the secretion of the two proteins in distinct subcellular
428 compartments, could be part of the immune priming processes. Two PME-related DAMPs, OGs and
429 MeOH are known to trigger defensive priming in plant immunity (Dorokhov et al., 2012; Komarova et
430 al., 2014; Gamir et al., 2021; Giovannoni et al., 2021). The possibility that SBTs, trigger PMEs to assist
431 and reinforce the OGs and MeOH signalling in priming is an interesting hypothesis to be investigated.
432 It is conceivable that the proteolytic cleavage of other Pro-proteins by these and other SBTs could
433 participate to trigger the immune response.
434 In conclusion, this study brings new insights into the molecular mechanisms underlying the activation
435 of PME related immunity against necrotrophs increasing our understanding of the complexity of the
436 interactions between plants and microbes. A switch on mechanism, mediated by SBTs for fine tuning
437 PME activity and pectin integrity signaling, emerges providing knowledge about how plants modulate
438 immunity. We identify Pro-PMEs as the target substrate processed by SBT3.3 indicating how this host
439 factor mediates immune prime activation. Future studies will be useful to identify the specific SBT-
440 Pro-PME pairs and to quantify the contribution of PME activity to priming. Activation of Pro-PMEs

441 and plant immunity by SBTs processing becomes an effective genomic tool to engineer durable, broad-
442 spectrum plant disease resistance and to avoid a growth-defense trade-offs.
443

444 **Materials And Methods**

445 **Plant, Bacteria and Fungus growth conditions**

446 *Arabidopsis thaliana* Wild-type Columbia (Col-0), *sbt* mutants and SBT3.3-OE seedlings were grown
447 in solid MS/2 medium [Murashige and Skoog Medium including vitamins (2.2 g L^{-1}), 1% sucrose,
448 0.8% plant agar, pH 5.7] in a controlled environmental chamber maintained at 22°C and 70% relative
449 humidity, with a 16h/8h day/night cycle (PAR level of 100 µmol $m^{-2}s^{-1}$). Adult plants were transferred
450 on soil in a growth chamber at 22°C and 70% relative humidity under a 12 h/12h day/night cycle (PAR
451 level of 120 µmol $m^{-2}s^{-1}$). *Sbt* mutants used include SALK_086092 (At1g32960; *sbt3.3-1*),
452 SALK_107460 (At1g32960; *sbt3.3-2*), SAIL_400_F09 (At1g32940; *sbt3.5-1*) and GABI_672C08
453 (At1g32940; *sbt3.5-2*). All mutants are in Col-0 background and are T-DNA insertion lines obtained
454 from the Nottingham *Arabidopsis* Stock Centre (NASC). *Nicotiana tabacum cv* SR1 seeds were
455 sterilized using commercial grade bleach solution in the presence of 0.1% (v/v) for 15 min at room
456 temperature and then washed three times for 5 min with distilled water before sowing. The seeds were
457 germinated in a growth room at 25°C and 30% relative humidity under a 16h/8h day/night cycle
458 (photosynthetic photon flux of 50 µmol $m^{-2}s^{-1}$). Three- to four-week-old plants from MS medium were
459 transferred on soil and grown in a controlled-environment at 25°C and 40% relative humidity under a
460 16h/8h day/night cycle (photosynthetic photon flux of 120 µmol $m^{-2}s^{-1}$). *Escherichia coli* TOP10 cells
461 was grown in LB agar plate (Luria-Bertani: tryptone 1%, yeast exctract 0.5%, NaCl 1%) containing
462 ampicillin 50µg/ml and incubated overnight at 37°C. *Agrobacterium tumefaciens* (Strain GV3110) was
463 grown in LB medium (Luria-Bertani: tryptone 1%, yeast exctract 0.5%, NaCl 1%) containing
464 appropriate antibiotics (Rifampycin 100µg/ml and Spectomycin 100µg/ml or Kanamycin 50µg/ml) and
465 incubated for 2 days at 28°C. *Botrytis cinerea* strain SF1 (Lionetti et al., 2007) was grown for 20 days
466 on Malt Extract Agar at 20 g L^{-1} with Mycological Peptone at 10 g L^{-1} (MEP) at 23°C and 70% relative
467 humidity in the dark before conidia collection.

468 For seed germination analysis, *A. thaliana* WT, *sbt* mutants and SBT3.3-OE seeds were washed in 2
469 mL of isopropanol for 30 seconds followed by washing in 2 mL of sterile water for 3 min in slow
470 agitation. Seeds were treated with 2 mL of sterilization solution (400 µl NaClO, 1.6 ml sterile water)
471 for 5 min in slow agitation, followed by 4 washing steps in 2 ml of sterile water. For seed germination
472 assay, triplicate sets of 60–70 sterilized seeds for each genotype were sown in Petri dishes on solid

473 MS/2 medium in a controlled environmental chamber maintained at 22°C and 70% relative humidity,
474 with a 16h/8h day/night cycle (PAR level of 100 µmol m-2s-1). Seeds germination rate, as the number
475 of germinated seeds divided by the total amount of total seeds, were scored at 24, 48 and 72 hours.
476
477 **Genotyping of T-DNA insertion mutants**
478 Genomic DNA was extracted using RBC Bioscience Genomic DNA Extraction Kits, according to the
479 manufacturer's instructions, from leaves of 4-week-old *Arabidopsis* wild-type and mutant plants and
480 subjected to a PCR-based screening using sequences of primer, described in Supplemental Table S1,
481 generated with Primer3 (https://primer3.ut.ee/). Taq Kapa DNA Polymerase (Kapa Biosystem) was
482 used at 1 units/30 µl of assay. Amplification was carried out in presence of dNTPs (0.2 mM), 2.5 mM
483 $MgCl_2$ and specific primers (10 µM) in the 1x buffer provide by the supplier. Conditions for
484 amplification were: 95°C for 3 minutes; 36 cycles of amplification: 95°C for 30 sec, 60°C for 30 sec,
485 72°C for 60 sec, and a final extension of 72°C for 1 min. PCR products were separated by agarose gel
486 electrophoresis and visualized by ethidium bromide staining. Plants homozygous for the mutations
487 were propagated and used for all subsequent experiments.
488
489 **Stable transformation of SBT3.3-OE *Arabidopsis* plants**
490 Flowering *Arabidopsis* plants were transformed by floral dipping for 15 seconds in 200 mL of the
491 culture medium with the inoculum of *Agrobacterium tumefaciens* C58 carrying the construction of
492 interest. The plants were subsequently covered for 1 day to promote the infection. The culture medium
493 for immersion was composed of MS 2.2 g/L and sucrose 5% (p/v), supplemented with Silwet 0.005%
494 and BAP 0.05 ug/mL. Subsequently, the selection of homozygous transgenic plants for the *SBT3.3-*
495 *YFP* construction was carried out by means of selection with BASTA herbicide.
496
497 **Elicitor Treatment and Gene expression analysis**
498 *B. cinerea*-infected or Mock-inoculated leaves were frozen in liquid nitrogen and homogenized using
499 the mixer mill MM301 (RETSCH) and using inox beads (5 mm diameter) for about 1 min at 30 Hz,
500 and total RNA was extracted with Isol-RNA Lysis Reagent (5′-Prime) according to the manufacturer's
501 instructions. RNA was treated with RQ1 DNase (Promega), and first-strand complementary DNA
502 (cDNA) was synthesized using ImProm-II reverse transcriptase (Promega). Quantitative Reverse
503 Transcription PCR analysis was performed using a CFX96 Real-Time System (Bio-Rad). One
504 microliter of cDNA (corresponding to 50 ng of total RNA) was amplified in 20 µL of reaction mix

505 containing 1× Go Taq qPCR Master Mix (Promega) and 0.5 µM of each primer described in
506 Supplemental Table S2. Conditions for amplification were: 95°C for 2 minutes; 46 cycles of
507 amplification: 95°C for 15 sec, 58°C for 15 sec, and a final extension of 72°C for 15 sec. Expression
508 levels of each gene, relative to the UBIQUITIN5 (UBQ5) gene, were determined using a modification
509 of the Pfaffl method (Pfaffl, 2001). Primer sequences were generated with Primer3 software
510 (https://primer3.ut.ee/). Seedlings of 10-days-old *Arabidopsis* cultured in liquid MS/2 medium were
511 treated for 1h with OG_S (40 µg mL^{-1}) or water as a control, collected and processed for RNA extraction
512 as described above.
513
514 ***Arabidopsis thaliana* infection with *Botrytis cinerea***
515 Conidia of *B. cinerea* were harvested by washing the surface of the mycelium with sterile distilled
516 water. Conidia suspensions were filtered to remove residual mycelium and the conidia concentration
517 was determined using a Thoma chamber. Fully developed leaves from 4-week-old *A. thaliana* plants
518 were infected with $1x10^6$ conidia mL^{-1} incubated in Potato Dextrose Broth (PDB) at 24 g L^{-1}. Six
519 droplets of spore suspension (5 µL each) were placed on the surface of each leaf. Mock-inoculation
520 was performed using PDB. Plants were incubated at 24°C with a 12h/12h day/night photoperiod. The
521 lesion size produced by *B. cinerea* was evaluated as an indicator of susceptibility to the fungus.
522
523 **Determination of PME activity, fungal diffusion and H_2O_2 accumulation**
524 Total protein extracts were obtained by homogenizing uninfected and infected *Arabidopsis* leaves in
525 the presence of 1M NaCl, 12.5 mM Citric Acid, 50 mM Na_2HPO_4, 0.02 % Sodium Azide, protease
526 inhibitor 1:200 v/v (P8849, Sigma), pH 6.5. Each sample was resuspended in 500 µL of protein
527 Extraction Buffer. The homogenates were shaken for 3 h at 4°C, centrifuged at 13.000 x g for 15 min,
528 and the supernatant (400 µL) collected. Protein concentration was determined in the supernatants using
529 Bradford protein assay method (Bradford reagent, Sigma–Aldrich), a standard curve was performed
530 using BSA (bovin serum albumine) at 1 mg mL^{-1}. PME activity was evaluated by using
531 PECTOPLATE assay (Lionetti, 2015): PECTOPLATE was prepared with 0.1% (w/v) of apple pectin
532 (molecular weight range 30,000–100,000 Da; 70–75% esterification; 76282, Sigma-Aldrich, St. Louis),
533 1% (w/v) SeaKem® LE agarose (Lonza, Basel, Switzerland, Catalog no: 50004E), 12.5 mM citric acid
534 and 50 mM Na_2HPO_4, pH 6.5. Equal amounts of protein samples (2 µg of total protein in 20 µL) were
535 loaded in each well of PECTOPLATE. Plates were incubated at 30°C for 16 h, and stained with 0.05%
536 (w/v) Ruthenium Red (RR) (R2751; Sigma-Aldrich, St. Louis) for 30 min. The plates were de-stained

537 by several washes with water and the area of the fuchsia-stained haloes, resulting from de-
538 methylesterification of pectin and the area of inner unstained haloes, resulting from the hydrolysis of
539 pectin in the gel, were measured with ImageJ software (Abramoff, Magalhes, and am 2004). Known
540 amounts of commercially available PME from orange (Citrus spp.) peel (P5400; Sigma-Aldrich) was
541 used in the PECTOPLATE to generate a standard curve used to calculate PME activity in the protein
542 extracts.
543 For the detection of *B. cinerea* hyphae, detached leaves were incubated for 30 min in lactophenol
544 Trypan Blue solution (water: glycerol: lactic acid: phenol [1:1:1:1] + Trypan Blue solution [1 mg mL^{-1};
545 Sigma-Aldrich]). Thereafter, leaves were washed for overnight with gentle agitation in absolute ethanol
546 to remove chlorophyll. Leaves were assayed for H_2O_2 accumulation employing 3,3′-diaminobenzidine
547 staining as previously described (Daudi and O'Brien, 2012). Leaves were mounted in 50% glycerol and
548 examined by light microscopy using Nikon eclipse E200 microscope. Images were taken with a Nikon
549 Digital Sight DS-Fi1c camera
550
551 **Determination of Monosaccharide Composition of CW and MEOH quantification**
552 Extraction of alcohol-insoluble residue, CW monosaccharide composition and the determination of CW
553 methylesters were performed as previously described (Lionetti et al., 2017).
554
555 **SBT3.3-YFP and PME17-GFP/RFP Gene Constructs**
556 For the SBT3.3-YFP overexpressing construct, a full-length cDNA for SBT3.3 was amplified by PCR
557 using Pfu DNA polymerase (Stratagene, San Diego, CA) and specific primers, described in
558 Supplemental Table S3, including Gateway adapters: BP SBT3.3 FW and BP SBT3.3 RV and
559 recombined into pDONR207 using BP ClonaseMixII kit (Invitrogen). After sequencing, the construct
560 was recombined with pB7FWG2 destination vector (YFP in C-terminal) using LR ClonaseMixII kit
561 (Invitrogen) and introduced into *Arabidopsis* (*sbt3.3*) via Agrobacterium transformation.
562 For PME17-GFP/RFP overexpressing constructs, the full-length cDNA for PME17 was amplified by
563 PCR using *TakaRa* Ex Taq DNA polymerase (TAKARA, Kyoto), and specific primers flanked by
564 Gateway adapters, attB sequences, described in Supplemental Table S3. PCR amplified attB-flanked
565 DNA was recombined into pDONR221 using BP ClonaseMixII kit (Invitrogen). Specific pDESTs,
566 pK7FWG2 and pK7RWG2,0, were used for GFP and RFP fusion in C-terminus to obtain Pro-PME17-
567 GFP and Pro-PME17-RFP, respectively. All constructs were checked by sequencing (Eurofins
568 Genomics, https://eurofinsgenomics.eu/). The Gateway constructs (Pro-PME17-GFP, Pro-PME17-RFP,

569 SBT3.3-YFP, SBT3.3-mCherry) and RFP-HDEL, ST52-mCherry, XTH11-RFP, pm-rk and Exo70E2-
570 mCherry were introduced into *Agrobacterium tumefaciens* (Strain GV3110) and the agroinfiltration
571 was performed in *Nicotiana tabacum* leaves as previously described (De Caroli et al., 2011).
572
573 **Transient transformation of *Nicotiana tabacum* leaves and confocal Laser Scanning Microscopy**
574 Almost fully expanded *Nicotiana tabacum* 6-week-old leaves were infiltrated with a suspension of
575 *Agrobacterium tumefaciens* bearing the relevant construct in 2mM Na3PO4; 50mM 2-(N-morpholine)-
576 ethanesulphonic acid (MES); glucose 0.5%; acetosyringone 100µM; pH= 5.6 at an OD_{600}=0.5. After 48
577 and 52 hours post infiltration (hpi) fluorescence was analyzed in infiltrated leaves by confocal
578 microscopy. For co-infiltration, *Agrobacterium* cultures grown separately were adjusted to an
579 OD_{600}=0.5 and mixed prior to infiltration. For BFA (Sigma-Aldrich, http://www.sigmaaldrich.com)
580 treatment, disks (1 cm diameter) of transformed leaves were treated by immersion in a solution of BFA
581 at the final concentration of 100 µM, as reported by De Caroli et al. (2021). Plasmolysis was induced
582 by incubating leaf disks in 1 M NaCl hypertonic solution for 10 min. Transiently transformed tobacco
583 leaves were observed using a confocal laser scanning microscope LSM710 Zeiss
584 (http://www.zeiss.com) mounting material in water as previously described (De Caroli et al., 2011).
585 GFP and YFP were detected within the short 505–530 nm wavelength range, assigning the green color;
586 RFP and mCherry were detected within 560–615 nm, assigning the red color. Excitation wavelengths
587 of 488 and 543 nm were used. The laser power was set to a minimum and appropriate controls were
588 made to ensure there was no bleed-through from one channel to the other. Images were processed using
589 PHOTOSHOP7.0 (Adobe, https://www.adobe.com). For quantitative colocalization analyses, the
590 overlap coefficient (OC, after Manders) and the Pearson's correlation coefficient (R) were evaluated as
591 previously reported (De Caroli et al., 2011).
592
593 **Bioinformatics tools**
594 The Expression Angler tool of the Bio-Analytic Resource for Plant Biology (BAR,
595 http://bar.utoronto.ca/welcome.htm) was used for co-expression analysis. E-plant
596 (https://bar.utoronto.ca/eplant/) was used for to study developmental map and biotic stresses. Chromas
597 was used to manage both nucleotide sequences and amino acids
598 (https://chromas.software.informer.com/2.5/). Primer3 (https://primer3.ut.ee/) was used to design
599 primers respectively for Gene expression analysis and Genotyping analysis. ImageJ was used to
600 calculate the area of the haloes in PECTOPLATE assay (http://imagej.nih.gov/ij/download.html).

601 DNAMAN software (Lynnon, BioSoft, Quebec, Canada, https://www.lynnon.com/) was used for
602 amino acid sequence analyses. Genevestigator Meta-Analyzer Tools (www.genevestigator.ethz.ch/at/)
603 was used to analyze *SBT3.3* and *SBT3.5* gene expression during infection of *Arabidopsis* with different
604 pathogens and DAMPs and PAMPs treatments.
605
606 **Accession numbers**
607 The genes used in this study have the following accession numbers: SBT3.3, At1g32960; SBT3.5,
608 At1g32940; UBQ5, At3g62250; PAD3, At3g26830; CYP81F2, At5g57220; PME17, At2g45220;
609 PMEI10, At1g62760; WAK2, At1G21270; At2g38470, WRKY33. *B. cinerea* β-tubulin,
610 MG949129.1.
611
612 **Supplemental data**
613 **Supplemental Figure S1.** Gene structure and alignment of amino acid sequences of Pro-PMEs induced
614 in Arabidopsis during *B. cinerea* infection.
615 **Supplemental Figure S2.** *SBT3.3* and *SBT3.5* gene expression in *Arabidopsis* challenged with *Botrytis*
616 *cinerea*.
617 **Supplemental Figure S3.** *SBT3.3* and *SBT3.5* gene expression during infection of *Arabidopsis* with
618 different pathogens and after different DAMPs and PAMPs treatments
619 **Supplemental Figure S4.** Seed morphology and germination are not altered in *sbt3.3*, *sbt3.5* mutants
620 and *SBT3.3*-OE lines.
621 **Supplemental Figure S5**. Arabidopsis *sbt3.3-1*, *sbt3.5-1* mutants and *SBT3.3-OE1* line are not
622 defective in H_2O_2 accumulation against *Botrytis*.
623 **Supplemental Table S1.** Primers used for genotyping
624 **Supplemental Table S2.** Primers used for qRT-PCR
625 **Supplemental Table S3.** Primers used to obtain Pro-PME17 and SBT3.3 fluorescent constructs with
626 Gateway system.
627
628 **Acknowledgments**
629 We thank Marco Greco for technical assistance.
630
631 **Funding**

The work was supported by Sapienza University of Rome, Grants RM120172B78CFDF2, RM11916B7A142CF1 and RG12117A898EABE0 to VL and AR12117A8A4A1ADC to DC and LV.

Author contributions

V.L. conceived the research; G.P, P.V and L.V. developed the experimental designs and supervised the experiments; D.C., D.D.C, M.O.M and M.D.C performed the experiments; D.C., M.D.C, G.P, P.V. and V.L. analysed data; All authors contributed to discussing the results of this manuscript. V.L. wrote the article with contributions of all the authors

642

643 # REFERENCES

644 **Abramoff MD, Magalh﹠es PJ, am SJ** (2004) Image processing with ImageJ. Biophotonics international **11**: 36–
645 42

646 **AbuQamar S, Moustafa K, Tran LS** (2017) Mechanisms and strategies of plant defense against Botrytis cinerea.
647 Critical Reviews in Biotechnology **37**: 262–274

648 **An SH, Sohn KH, Choi HW, Hwang IS, Lee SC, Hwang BK** (2008) Pepper pectin methylesterase inhibitor protein
649 CaPMEI1 is required for antifungal activity, basal disease resistance and abiotic stress tolerance. Planta
650 **228**: 61–78

651 **Bethke G, Grundman RE, Sreekanta S, Truman W, Katagiri F, Glazebrook J** (2014) Arabidopsis PECTIN
652 METHYLESTERASES Contribute to Immunity Against Pseudomonas syringae. Plant Physiol **164**: 1093–
653 1107

654 **Birkenbihl RP, Diezel C, Somssich IE** (2012) Arabidopsis WRKY33 is a key transcriptional regulator of hormonal
655 and metabolic responses toward Botrytis cinerea infection. Plant Physiol **159**: 266–285

656 **Bosch M, Cheung AY, Hepler PK** (2005) Pectin Methylesterase, a Regulator of Pollen Tube Growth. Plant
657 Physiol **138**: 1334–1346

658 **Bruce TJA, Matthes MC, Napier JA, Pickett JA** (2007) Stressful “memories” of plants: Evidence and possible
659 mechanisms. Plant Science **173**: 603–608

660 **Brutus A, Sicilia F, Macone A, Cervone F, De Lorenzo G** (2010) A domain swap approach reveals a role of the
661 plant wall-associated kinase 1 (WAK1) as a receptor of oligogalacturonides. Proc Natl Acad Sci USA **107**:
662 9452–9457

663 **de la Canal L, Pinedo M** (2018) Extracellular vesicles: a missing component in plant cell wall remodeling.
664 Journal of Experimental Botany **69**: 4655–4658

665 **Clay NK, Adio AM, Denoux C, Jander G, Ausubel FM** (2009) Glucosinolate metabolites required for an
666 Arabidopsis innate immune response. Science **323**: 95–101

667 **Coculo D, Lionetti V** (2022) The Plant Invertase/Pectin Methylesterase Inhibitor Superfamily. Frontiers in Plant
668 Science **13**: 863892

669 **Conrath U** (2011) Molecular aspects of defence priming. Trends in Plant Science **16**: 524–531

670 **Daudi A, O’Brien JA** (2012) Detection of Hydrogen Peroxide by DAB Staining in Arabidopsis Leaves. Bio Protoc
671 **2**: e263

672 **De Caroli M, Lenucci MS, Di Sansebastiano GP, Dalessandro G, De Lorenzo G, Piro G** (2011) Protein trafficking
673 to the cell wall occurs through mechanisms distinguishable from default sorting in tobacco. Plant J **65**:
674 295–308

675 **De Caroli M, Lenucci MS, Manualdi F, Dalessandro G, De Lorenzo G, Piro G** (2015) Molecular dissection of
676 Phaseolus vulgaris polygalacturonase-inhibiting protein 2 reveals the presence of hold/release domains
677 affecting protein trafficking toward the cell wall. Front.Plant Sci. 6:

678 **De Caroli M, Manno E, Piro G, Lenucci MS** (2021) Ride to cell wall: Arabidopsis XTH11, XTH29 and XTH33
679 exhibit different secretion pathways and responses to heat and drought stress. The Plant Journal **107**:
680 448–466

681 **Dean R, van Kan JAL, Pretorius ZA, Hammond-Kosack KE, Di Pietro A, Spanu PD, Rudd JJ, Dickman M,**
682 **Kahmann R, Ellis J, et al** (2012) The Top 10 fungal pathogens in molecular plant pathology. MolPlant
683 Pathol **13**: 414–430

684 **Decreux A, Messiaen J** (2005) Wall-associated kinase WAK1 interacts with cell wall pectins in a calcium-induced
685 conformation. Plant Cell Physiol **46**: 268–278

686 **Dedeurwaerder S, Menu-Bouaouiche L, Mareck A, Lerouge P, Guerineau F** (2008) Activity of an atypical
687 Arabidopsis thaliana pectin methylesterase. Planta **229**: 311–21

688 **Del Corpo D, Fullone MR, Miele R, Lafond M, Pontiggia D, Grisel S, Kieffer-Jaquinod S, Giardina T, Bellincampi**
689 **D, Lionetti V** (2020) AtPME17 is a functional Arabidopsis thaliana pectin methylesterase regulated by
690 its PRO region that triggers PME activity in the resistance to Botrytis cinerea. Molecular Plant Pathology
691 **21**: 1620–1633

692 **Denoux C, Galletti R, Mammarella N, Gopalan S, Werck D, De Lorenzo G, Ferrari S, Ausubel FM, Dewdney J**
693 (2008) Activation of defense response pathways by OGs and Flg22 elicitors in Arabidopsis seedlings.
694 Mol Plant **1**: 423–445

695 **Doehlemann G, Hemetsberger C** (2013) Apoplastic immunity and its suppression by filamentous plant
696 pathogens. New Phytologist **198**: 1001–1016

697 **Dorokhov YL, Komarova TV, Petrunia IV, Frolova OY, Pozdyshev DV, Gleba YY** (2012) Airborne Signals from a
698 Wounded Leaf Facilitate Viral Spreading and Induce Antibacterial Resistance in Neighboring Plants. Plos
699 Pathogens 8:

700 **Engelsdorf T, Gigli-Bisceglia N, Veerabagu M, McKenna JF, Vaahtera L, Augstein F, Does DV der, Zipfel C,**
701 **Hamann T** (2018) The plant cell wall integrity maintenance and immune signaling systems cooperate to
702 control stress responses in Arabidopsis thaliana. Sci Signal **11**: eaao3070

703 **Feng W, Kita D, Peaucelle A, Cartwright HN, Doan V, Duan Q, Liu M-C, Maman J, Steinhorst L, Schmitz-Thom**
704 **I, et al** (2018) The FERONIA Receptor Kinase Maintains Cell-Wall Integrity during Salt Stress through
705 Ca2+ Signaling. Curr Biol **28**: 666-675.e5

706 **Ferrari S, Savatin DV, Sicilia F, Gramegna G, Cervone F, De Lorenzo G** (2013) Oligogalacturonides: plant
707 damage-associated molecular patterns and regulators of growth and development. Front.Plant Sci. doi:
708 10.3389/fpls.2013.00049:

709 **Figueiredo A, Monteiro F, Sebastiana M** (2014) Subtilisin-like proteases in plant-pathogen recognition and
710 immune priming: a perspective. FrontPlant Sci **5**: 739.

711 **Figueiredo J, Sousa Silva M, Figueiredo A** (2018) Subtilisin-like proteases in plant defence: the past, the
712 present and beyond: Subtilases in plant defence. Molecular Plant Pathology **19**: 1017–1028

713 **Gamir J, Minchev Z, Berrio E, García JM, De Lorenzo G, Pozo MJ** (2021) Roots drive oligogalacturonide-induced
714 systemic immunity in tomato. Plant, Cell & Environment **44**: 275–289

715 **Geilfus C-M** (2017) The pH of the Apoplast: Dynamic Factor with Functional Impact Under Stress. Mol Plant **10**:
716 1371–1386

717 **Giovannoni M, Lironi D, Marti L, Paparella C, Vecchi V, Gust AA, De Lorenzo G, Nürnberger T, Ferrari S** (2021)
718 The Arabidopsis thaliana LysM-containing Receptor-Like Kinase 2 is required for elicitor-induced
719 resistance to pathogens. Plant, Cell & Environment **44**: 3775–3792

720 **Godson A, van der Hoorn RAL** (2021) The front line of defence: a meta-analysis of apoplastic proteases in plant
721 immunity. Journal of Experimental Botany **72**: 3381–3394

722 **Guo H, Nolan TM, Song G, Liu S, Xie Z, Chen J, Schnable PS, Walley JW, Yin Y** (2018) FERONIA Receptor Kinase
723 Contributes to Plant Immunity by Suppressing Jasmonic Acid Signaling in Arabidopsis thaliana. Curr Biol
724 **28**: 3316-3324.e6

725 **Ha CM, Rao X, Saxena G, Dixon RA** (2021) Growth–defense trade-offs and yield loss in plants with engineered
726 cell walls. New Phytologist **231**: 60–74

727 **Hann CT, Bequette CJ, Dombrowski JE, Stratmann JW** (2014) Methanol and ethanol modulate responses to
728 danger- and microbe-associated molecular patterns. Front.Plant Sci. 5:

729 **He Z, Webster S, He SY** (2022) Growth-defense trade-offs in plants. Curr Biol **32**: R634–R639

730 **Hohl M, Stintzi A, Schaller A** (2017) A novel subtilase inhibitor in plants shows structural and functional
731 similarities to protease propeptides. J Biol Chem **292**: 6389–6401

732 **Hou S, Jamieson P, He P** (2018) The cloak, dagger, and shield: proteases in plant–pathogen interactions.
733 Biochemical Journal **475**: 2491–2509

734 **Huot B, Yao J, Montgomery BL, He SY** (2014) Growth–Defense Tradeoffs in Plants: A Balancing Act to Optimize
735 Fitness. Molecular Plant **7**: 1267–1287

736 **Janzik I, Macheroux P, Amrhein N, Schaller A** (2000) LeSBT1, a Subtilase from Tomato Plants:
737 OVEREXPRESSION IN INSECT CELLS, PURIFICATION, AND CHARACTERIZATION*. Journal of Biological
738 Chemistry **275**: 5193–5199

739 **Khan AR, James MN** (1998) Molecular mechanisms for the conversion of zymogens to active proteolytic
740 enzymes. Protein Sci **7**: 815–836

741 **Kohorn BD, Kohorn SL** (2012) The cell wall-associated kinases, WAKs, as pectin receptors. FrontPlant Sci **3**: 88

742 **Kohorn BD, Kohorn SL, Saba NJ, Martinez VM** (2014) Requirement for Pectin Methyl Esterase and Preference
743 for Fragmented over Native Pectins for Wall-associated Kinase-activated, EDS1/PAD4-dependent Stress
744 Response in Arabidopsis. JBiolChem **289**: 18978–18986

745 **Komarova TV, Sheshukova EV, Dorokhov YL** (2014) Cell wall methanol as a signal in plant immunity.
746 Front.Plant Sci. 5:

747 **Lichtenthaler SF, Lemberg MK, Fluhrer R** (2018) Proteolytic ectodomain shedding of membrane proteins in
748 mammals—hardware, concepts, and recent developments. EMBO J **37**: e99456

749 **Lin W, Tang W, Anderson CT, Yang Z** (2018) FERONIA's sensing of cell wall pectin activates ROP GTPase
750 signaling in Arabidopsis. bioRxiv 269647

751 **Lin W, Tang W, Pan X, Huang A, Gao X, Anderson CT, Yang Z** (2021) Arabidopsis pavement cell morphogenesis
752 requires FERONIA binding to pectin for activation of ROP GTPase signaling. Current Biology
753 S096098222101589X

754 **Lionetti V** (2015) PECTOPLATE: the simultaneous phenotyping of pectin methylesterases, pectinases, and
755 oligogalacturonides in plants during biotic stresses. FrontPlant Sci **6**: 1–8

756 **Lionetti V, Cervone F, Bellincampi D** (2012) Methyl esterification of pectin plays a role during plant-pathogen
757 interactions and affects plant resistance to diseases. JPlant Physiol **169**: 1623–1630

758 **Lionetti V, Fabri E, De Caroli M, Hansen AR, Willats WG, Piro G, Bellincampi D** (2017) Three pectin methyl
759 esterase inhibitors protect cell wall integrity for immunity to Botrytis. Plant Physiol **Jan 12.**: pii:
760 pp.01185.2016.

761 **Lionetti V, Francocci F, Ferrari S, Volpi C, Bellincampi D, Galletti R, D'Ovidio R, De Lorenzo G, Cervone F** (2010)
762 Engineering the cell wall by reducing de-methyl-esterified homogalacturonan improves saccharification
763 of plant tissues for bioconversion. Proc Natl Acad Sci USA **107**: 616–621

764 **Lionetti V, Raiola A, Camardella L, Giovane A, Obel N, Pauly M, Favaron F, Cervone F, Bellincampi D** (2007)
765 Overexpression of Pectin Methylesterase Inhibitors in Arabidopsis Restricts Fungal Infection by Botrytis
766 cinerea. Plant Physiol **143**: 1871–1880

767 **Lionetti V, Raiola A, Cervone F, Bellincampi D** (2014) Transgenic expression of pectin methylesterase inhibitors
768 limits tobamovirus spread in tobacco and Arabidopsis. MolPlant Pathol **15**: 265–274

769 **Liu N, Sun Y, Pei Y, Zhang X, Wang P, Li X, Li F, Hou Y** (2018) A Pectin Methylesterase Inhibitor Enhances
770 Resistance to Verticillium Wilt1[OPEN]. Plant Physiol **176**: 2202–2220

771 **Lozano-Torres JL, Wilbers RHP, Warmerdam S, Finkers-Tomczak A, Diaz-Granados A, Schaik CC van, Helder J,**
772 **Bakker J, Goverse A, Schots A, et al** (2014) Apoplastic Venom Allergen-like Proteins of Cyst Nematodes
773 Modulate the Activation of Basal Plant Innate Immunity by Cell Surface Receptors. PLOS Pathogens **10**:
774 e1004569

775 **Meyer M, Huttenlocher F, Cedzich A, Procopio S, Stroeder J, Pau-Roblot C, Lequart-Pillon M, Pelloux J, Stintzi**
776 **A, Schaller A** (2016) The subtilisin-like protease SBT3 contributes to insect resistance in tomato. EXBOTJ
777 **67**: 4325–4338

778 **Nelson BK, Cai X, Nebenfuhr A** (2007) A multicolored set of in vivo organelle markers for co-localization studies
779 in Arabidopsis and other plants. Plant J **51**: 1126–1136

780 **Ogawa S, Wakatake T, Spallek T, Ishida JK, Sano R, Kurata T, Demura T, Yoshida S, Ichihashi Y, Schaller A, et al**
781 (2021) Subtilase activity in intrusive cells mediates haustorium maturation in parasitic plants. Plant
782 Physiology **185**: 1381–1394

783 **Osorio S, Bombarely A, Giavalisco P, Usadel B, Stephens C, Araguez I, Medina-Escobar N, Botella MA, Fernie**
784 **AR, Valpuesta V** (2011) Demethylation of oligogalacturonides by FaPE1 in the fruits of the wild
785 strawberry Fragaria vesca triggers metabolic and transcriptional changes associated with defence and
786 development of the fruit. JExpBot **62**: 2855–2873

787 **Osorio S, Castillejo C, Quesada MA, Medina-Escobar N, Brownsey GJ, Suau R, Heredia A, Botella MA,**
788 **Valpuesta V** (2008) Partial demethylation of oligogalacturonides by pectin methyl esterase 1 is
789 required for eliciting defence responses in wild strawberry (Fragaria vesca). Plant J **54**: 43–55

790 **Paulus JK, Van der Hoorn RAL** (2019) Do proteolytic cascades exist in plants? Journal of Experimental Botany
791 **70**: 1997–2002

792 **Pelloux J, Rustérucci C, Mellerowicz EJ** (2007) New insights into pectin methylesterase structure and function.
793 Trends Plant Sci **12**: 267–277

794 **Pogorelko G, Lionetti V, Fursova O, Sundaram RM, Qi MS, Whitham SA, Bogdanove AJ, Bellincampi D,**
795 **Zabotina OA** (2013) Arabidopsis and Brachypodium distachyon Transgenic Plants Expressing Aspergillus
796 nidulans Acetylesterases Have Decreased Degree of Polysaccharide Acetylation and Increased
797 Resistance to Pathogens. Plant Physiol **162**: 9–23

798 **Ramirez V, Lopez A, Mauch-Mani B, Gil MJ, Vera P** (2013) An Extracellular Subtilase Switch for Immune
799 Priming in Arabidopsis. Plos Pathogens 9:

800 **Rautengarten C, Steinhauser D, Bussis D, Stintzi A, Schaller A, Kopka J, Altmann T** (2005) Inferring Hypotheses
801 on Functional Relationships of Genes: Analysis of the Arabidopsis thaliana Subtilase Gene Family.
802 PLoS.Comput.Biol. 1:

803 **Rautengarten C, Usadel B, Neumetzler L, Hartmann J, Büssis D, Altmann T** (2008) A subtilisin-like serine
804 protease essential for mucilage release from Arabidopsis seed coats. The Plant Journal **54**: 466–480

805 **Reem N, Pogorelko G, Lionetti V, Chambers L, Held MA, Bellincampi D, Zabotina OA** (2016) Decreased
806 polysaccharide feruloylation compromises plant cell wall integrity and increases susceptibility to
807 necrotrophic fungal pathogens. FrontPlant Sci **7**: 630, doi: 10.3389/fpls.2016.00630

808 **Reichardt S, Repper D, Tuzhikov AI, Galiullina RA, Planas-Marquès M, Chichkova NV, Vartapetian AB, Stintzi**
809 **A, Schaller A** (2018) The tomato subtilase family includes several cell death-related proteinases with
810 caspase specificity. Sci Rep **8**: 10531

811 **Rosenfeld N, Elowitz MB, Alon U** (2002) Negative autoregulation speeds the response times of transcription
812 networks. J Mol Biol **323**: 785–793

813 **Schaller A** (2004) A cut above the rest: the regulatory function of plant proteases. Planta **220**: 183–197

814 **Schaller A, Stintzi A, Rivas S, Serrano I, Chichkova NV, Vartapetian AB, Martínez D, Guiamét JJ, Sueldo DJ, van**
815 **der Hoorn RAL, et al** (2018) From structure to function - a family portrait of plant subtilases. New
816 Phytol **218**: 901–915

817 **Senechal F, Graff L, Surcouf O, Marcelo P, Rayon C, Bouton S, Mareck A, Mouille G, Stintzi A, Hofte H, et al**
818 (2014a) Arabidopsis PECTIN METHYLESTERASE17 is co-expressed with and processed by SBT3.5, a
819 subtilisin-like serine protease. AnnBot **114**: 1161–1175

820 **Senechal F, Wattier C, Rusterucci C, Pelloux J** (2014b) Homogalacturonan-modifying enzymes: structure,
821 expression, and roles in plants. JExpBot **65**: 5125–5160

822 **Serrano I, Buscaill P, Audran C, Pouzet C, Jauneau A, Rivas S** (2016) A non canonical subtilase attenuates the
823 transcriptional activation of defence responses in Arabidopsis thaliana. eLife **5**: e19755

824 **Siegmund U, Viefhues A** (2016) Reactive Oxygen Species in the Botrytis – Host Interaction. *In* S Fillinger, Y Elad,
825 eds, Botrytis – the Fungus, the Pathogen and its Management in Agricultural Systems. Springer
826 International Publishing, Cham, pp 269–289

827 **Stegmann M, Monaghan J, Smakowska-Luzan E, Rovenich H, Lehner A, Holton N, Belkhadir Y, Zipfel C** (2017)
828 The receptor kinase FER is a RALF-regulated scaffold controlling plant immune signaling. Science **355**:
829 287–289

830 **Tornero P, Conejero V, Vera P** (1996) Primary structure and expression of a pathogen-induced protease (PR-
831 P69) in tomato plants: Similarity of functional domains to subtilisin-like endoproteases. Proceedings of
832 the National Academy of Sciences **93**: 6332–6337

833 **Vartapetian AB, Tuzhikov AI, Chichkova NV, Taliansky M, Wolpert TJ** (2011) A plant alternative to animal
834 caspases: subtilisin-like proteases. Cell Death Differ **18**: 1289–1297

835 **Wang J, Ding Y, Wang J, Hillmer S, Miao Y, Lo SW, Wang X, Robinson DG, Jiang L** (2010) EXPO, an Exocyst-
836 Positive Organelle Distinct from Multivesicular Endosomes and Autophagosomes, Mediates Cytosol to
837 Cell Wall Exocytosis in Arabidopsis and Tobacco Cells[C][W]. Plant Cell **22**: 4009–4030

838 **Wang S, Xing R, Wang Y, Shu H, Fu S, Huang J, Paulus JK, Schuster M, Saunders DGO, Win J, et al** (2021)
839 Cleavage of a pathogen apoplastic protein by plant subtilases activates host immunity. New Phytol **229**:
840 3424–3439

841 **Wang X, Chung KP, Lin W, Jiang L** (2017) Protein secretion in plants: conventional and unconventional
842 pathways and new techniques. J Exp Bot **69**: 21–37

843 **Williamson B, Tudzynski B, Tudzynski P, Kan J a. LV** (2007) Botrytis cinerea: the cause of grey mould disease.
844 Molecular Plant Pathology **8**: 561–580

845 **Wolf S, Rausch T, Greiner S** (2009) The N-terminal pro region mediates retention of unprocessed type-I PME in
846 the Golgi apparatus. The Plant Journal **58**: 361–375

847 **Wormit A, Usadel B** (2018) The Multifaceted Role of Pectin Methylesterase Inhibitors (PMEIs). Int J Mol Sci.
848 doi: 10.3390/ijms19102878

849 **Zhang H, Zhang L, Gao B, Fan H, Jin J, Botella MA, Jiang L, Lin J** (2011) Golgi Apparatus-Localized
850 Synaptotagmin 2 Is Required for Unconventional Secretion in Arabidopsis. PLOS ONE **6**: e26477

851 **Zhou J-M, Zhang Y** (2020) Plant Immunity: Danger Perception and Signaling. Cell **181**: 978–989

852 **Zhou N, Tootle TL, Glazebrook J** (1999) Arabidopsis PAD3, a gene required for camalexin biosynthesis, encodes
853 a putative cytochrome P450 monooxygenase. Plant Cell **11**: 2419–28

854

855 **Figure legends**

856 **Figure 1. *SBT3.3* and *SBT3.5* are induced in *Arabidopsis* during *B. cinerea* infection and SBT3.3**
857 **is induced by OGs treatment. A**) *SBT3.3* and **B)** *SBT3.5* expression was analysed in *B. cinerea*
858 infected or mock-inoculated leaves at the indicated hours post inoculation (hpi) by qPCR. M = Mock
859 inoculated leaves. B = *B. cinerea* inoculated leaves. The expression of **C)** *SBT3.3* and **D)** *SBT3.5* was
860 analysed in Arabidopsis WT seedlings after 1 hour of treatment with OGs or with water (H_2O) as a
861 control. The expression levels were normalized to *Ubiquitin5* expression. Data represent mean ± SD
862 (n=3). The experiments were repeated three times with similar results.

863

864 **Figure 2. Isolation of Arabidopsis *SBT3.3* and *SBT3.5* T-DNA insertional mutants. A)** Schematic
865 representation of *SBT3.3* and *SBT3.5* gene structures. The localization of T-DNA insertions in the gene
866 sequences are shown (black arrows). 5′-UTR and 3′-UTR are represented in grey, exons in white and
867 introns as a black line. **B)** The expression of *SBT3.3* and *SBT3.5* was analyzed in the respective mutants
868 and WT plants at 24-hour post inoculation with *B. cinerea*. The expression levels were normalized to
869 *Ubiquitin 5* expression. The experiments were repeated three times with similar results. **C)**
870 Representative pictures illustrating the morphology of vegetative rosettes of *sbt3.3* and *sbt3.5* mutants
871 compared with WT. **D)** The monosaccharide composition of cell wall matrix polysaccharides was
872 compared in leaves of *sbt3.3* and s*bt3.5* mutants and WT plants. The molar percentages of Fucose
873 (Fuc), Rhamnose (Rha), Arabinose (Ara), Galactose (Gal), Glucose (Glu), Xylose (Xyl), Mannose
874 (Man), Galacturonic Acid (Gal A) and Glucuronic Acid (Glc A) were quantified. The results represent
875 the mean ± SD (n≥3). Monosaccharide datasets are not significantly different according to analysis of
876 variance (ANOVA) followed by Tukey's test ($P < 0.05$).

877

878 **Figure 3. SBT3.3 and SBT3.5 regulate PME activity during disease. A)** Schematic representation of
879 the binding of Ruthenium Red to de-methylesterified pectin. **B)** Leaves of Arabidopsis WT and of *sbt*
880 mutants were inoculated with *Botrytis* and Mock and PME activity were quantified at 24-hour post
881 inoculation (hpi). The results represent the mean ± SD (n = 6). The different letters on the bars indicate
882 datasets significantly different according to ANOVA followed by Tukey's test ($P < 0.05$).

883

884 **Figure 4. The lack of *SBT3.3 and SBT3.5* expression reduces *Arabidopsis* resistance to *Botrytis***
885 ***cinerea*. A)** Quantification of lesion areas produced by the spreading of the fungus at 24 hours post
886 infections. Data represent mean ± SE (n ≥14 lesions for each genotype). Different letters indicate
887 statistically significant differences, according to ANOVA followed by Tukey's significance test ($P <$
888 0.05). **B)** Photographs showing lesion areas produced by *Botrytis* on leaves of Arabidopsis WT, *sbt3.3-*
889 *1 and sbt3.5-1* mutants (left) and microphotographs showing *Botrytis* colonization revealed by trypan
890 blue staining (right). Bars = 1mm.

891

892 **Figure 5. The *SBT3.3* overexpression in Arabidopsis does not alter rosette growth and cell wall**
893 **composition. A)** The expression of *SBT3.3* was analyzed in the *SBT3.3-OE1* and *SBT3.3-OE2*
894 transgenic plants at 24-hour post inoculation with Mock and *B. cinerea* spores. The expression levels
895 were normalized to *Ubiquitin5* expression. The experiments were repeated three times with similar
896 results. **B)** Representative pictures illustrating the morphology of vegetative rosettes of *SBT3.3*
897 overexpressing plants compared with WT plants. **C)** The molar percentages of Fucose (Fuc),
898 Rhamnose (Rha), Arabinose (Ara), Galactose (Gal), Glucose (Glu), Xylose (Xyl), Mannose (Man),
899 Galacturonic Acid (Gal A) and Glucuronic Acid (Glc A) were quantified. The results represent the
900 mean ± SD (n ≥ 3). Monosaccharide datasets are not significantly different according to analysis of
901 variance (ANOVA) followed by Tukey's test ($P < 0.05$).

902

903 **Figure 6. The *SBT3.3* overexpression overactivates PME activity restricting *Botrytis* infection. A)**
904 Leaves of Arabidopsis WT and of *SBT3.3-OE* plants were inoculated with *Botrytis* and Mock and PME
905 activity were quantified at 24-hour post inoculation. The results represent the mean ± SD (n = 6). **B)**
906 The amount of methylesters in the cell wall were quantified at 24-hour post inoculation. The results
907 represent the mean ± SD (n = 6). **C)** Quantification of lesion areas produced by the spreading of the
908 fungus at 24 hours post infections. Data represent mean ± SE (n≥15 lesions for each genotype). **D)**
909 Photographs showing lesion areas produced by *Botrytis* on leaves of WT and *SBT3.3-OE1* plants (left)
910 and microphotographs showing *Botrytis* colonization revealed by trypan blue staining. Bars = 1mm.
911 The different letters in A, B and C indicate datasets significantly different according to ANOVA
912 followed by Tukey's test ($P < 0.05$).

913

914 **Figure 7. *SBT3.3* overexpression enhances immune responces.** The induction of the expression of
915 defence genes *WRKY33, PAD3, WAK2, CYP81F2, PME17, PMEI10* were compared between *SBT3.3-*
916 *OE1* line and WT plants challenged with *Botrytis*. The mRNA expression was analysed at 24 hpi in *B.*
917 *cinerea-* or mock-inoculated leaves by qPCR. *Botrytis β-tubulin* expression was also quantified. The
918 expression levels were normalized to *Ubiquitin5* expression. The experiments were repeated three
919 times with similar results.
920
921 **Figure 8. SBT3.3 and Pro-PME17 are delivered in the apoplast through different protein**
922 **secretion pathways.**
923 Confocal microscopy images of epidermal cells of *Nicotiana tabacum* adult leaves showing the
924 coexpression of SBT3.3-YFP (**A-P**) or Pro-PME17-GFP (**Q-Z**) with different markers of subcellular
925 compartments (**B-C-, R-S:** XTH11-RFP, cell wall; **F-G, V-W** RFP-HDEL, endoplasmic reticulum; **I-J,**
926 **Y-Z:** ST52-mCherry, Golgi stacks) at the indicated hours post infiltration (hpi). Plasmolyzed cells (1 M
927 NaCl) expressing SBT3.3-YFP or Pro-PME17-GFP and the plasma membrane marker pm-rk show the
928 green fluorescent cell wall and the retracted red fluorescent plasma membrane (**D, T**). Chlorophyll
929 autofluorescence within the chloroplasts is depicted in blue. Scale bars = 20 µm (**A-C, Q-S**), 10 µm (**E-**
930 **P**, **U-Z**), and 5 µm (**D, T**).
931
932 **Figure 9. Pro-PME17 and SBT3.3 colocalize in the cell wall and their colocalization is favoured**
933 **over time.** Confocal microscopy images of epidermal cells of tobacco adult leaves co-expressing Pro-
934 PME17-RFP (**A** and **D**) and SBT3.3-YFP (**B** and **E**) at the indicated hours post infiltration (hpi).
935 Merged images showing the co-localization of SBT3.3-YFP and Pro-PME17-RFP in the cell wall (**C**
936 and **F**). Overlap coefficient (OC, after Manders) and R (Pearson's correlation coefficient) values are
937 reported in each merged image. Chlorophyll autofluorescence within the chloroplasts is depicted in
938 blue. Scale bars = 20 µm.

939

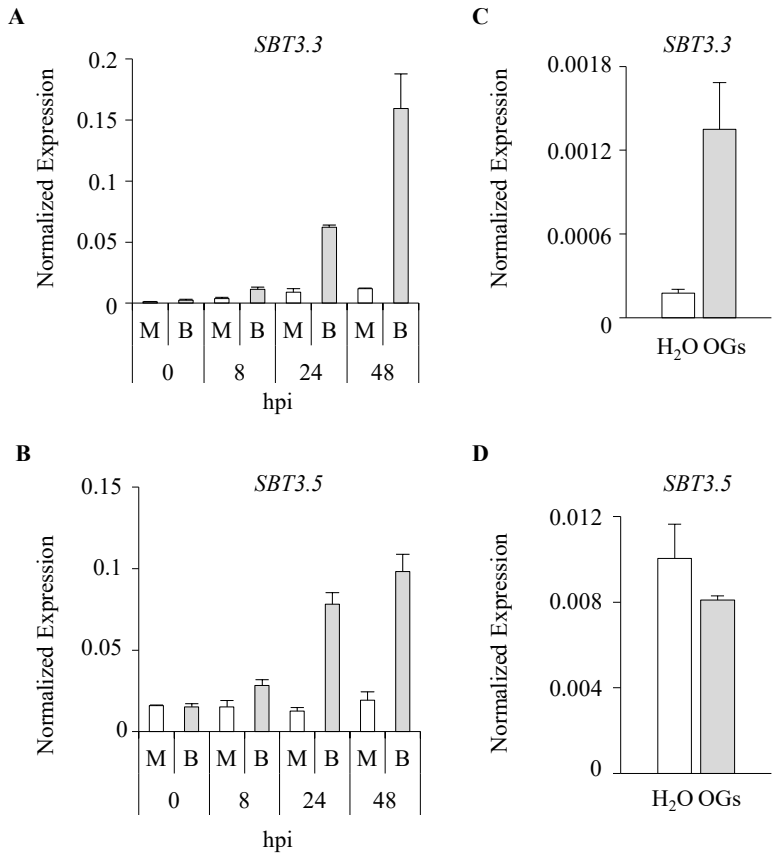

Figure 1. *SBT3.3* and *SBT3.5* are induced in *Arabidopsis* during *B. cinerea* infection and SBT3.3 is induced by OGs treatment. A) *SBT3.3* and **B)** *SBT3.5* expression was analysed in *B. cinerea* infected or mock-inoculated leaves at the indicated hours post inoculation (hpi) by qPCR. M = Mock inoculated leaves. B = *B. cinerea* inoculated leaves. The expression of **C)** *SBT3.3* and **D)** *SBT3.5* was analysed in Arabidopsis WT seedlings after 1 hour of treatment with OGs or with water (H_2O) as a control. The expression levels were normalized to *Ubiquitin5* expression. Data represent mean ± SD (n=3). The experiments were repeated three times with similar results.

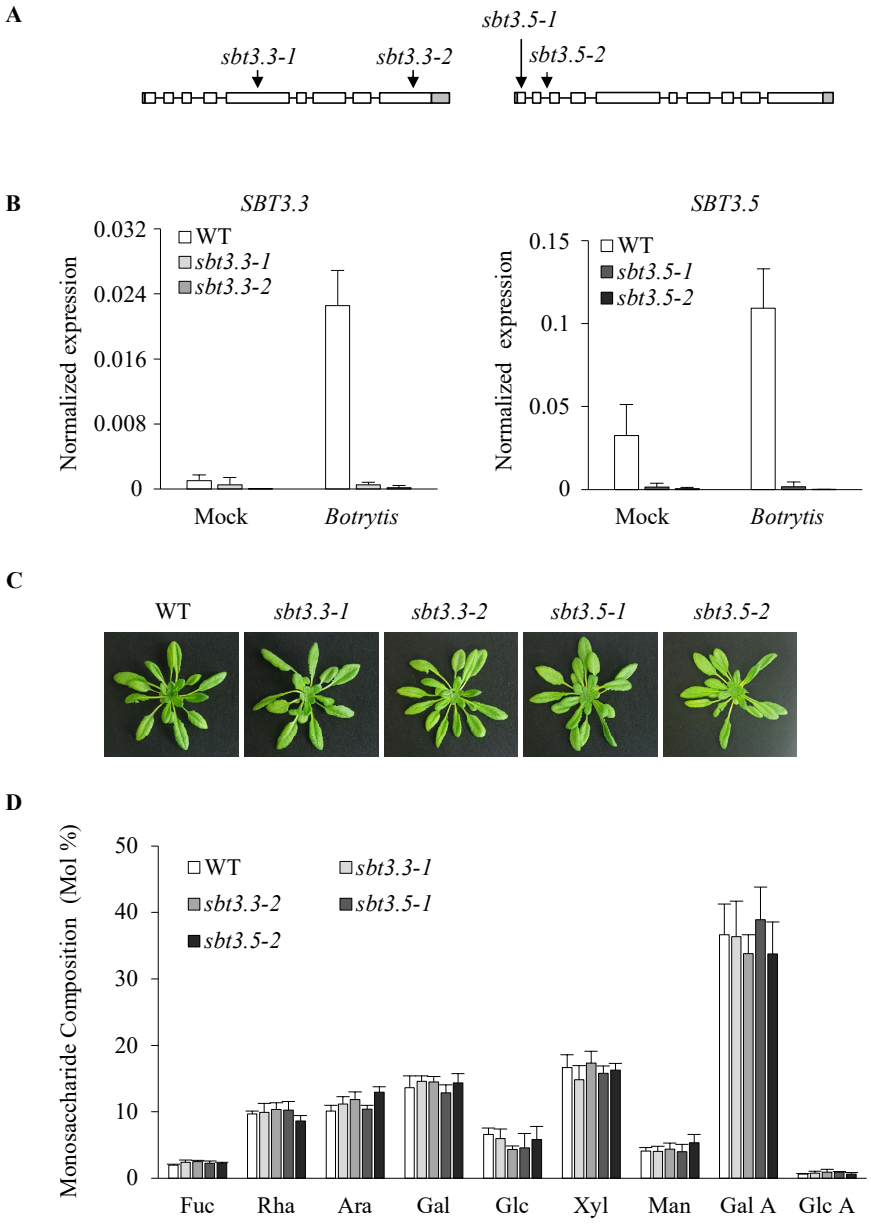

Figure 2. Isolation of Arabidopsis *SBT3.3* and *SBT3.5* T-DNA insertional mutants. A) Schematic representation of *SBT3.3* and *SBT3.5* gene structures. The localization of T-DNA insertions in the gene sequences are shown (black arrows). 5′-UTR and 3′-UTR are represented in grey, exons in white and introns as a black line. **B)** The expression of *SBT3.3* and *SBT3.5* was analyzed in the respective mutants and WT plants at 24-hour post inoculation with *B. cinerea*. The expression levels were normalized to *Ubiquitin 5* expression. The experiments were repeated three times with similar results. **C)** Representative pictures illustrating the morphology of vegetative rosettes of *sbt3.3* and *sbt3.5* mutants compared with WT. **D)** The monosaccharide composition of cell wall matrix polysaccharides was compared in leaves of *sbt3.3* and s*bt3.5* mutants and WT plants. The molar percentages of Fucose (Fuc), Rhamnose (Rha), Arabinose (Ara), Galactose (Gal), Glucose (Glu), Xylose (Xyl), Mannose (Man), Galacturonic Acid (Gal A) and Glucuronic Acid (Glc A) were quantified. The results represent the mean ± SD (n≥3). Monosaccharide datasets are not significantly different according to analysis of variance (ANOVA) followed by Tukey's test ($P < 0.05$).

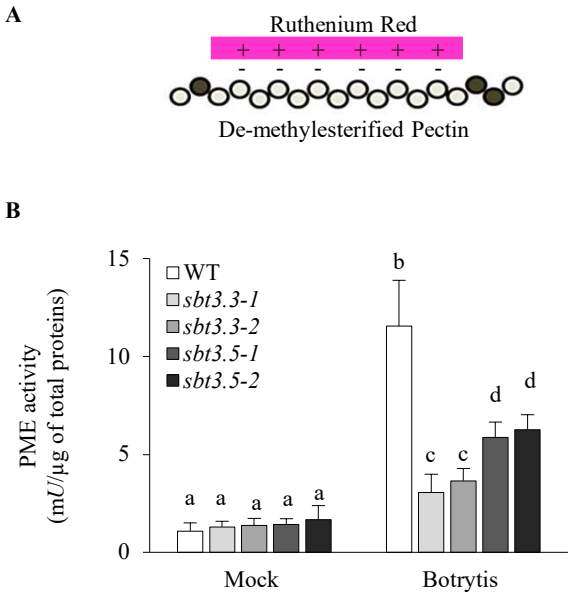

Figure 3. SBT3.3 and SBT3.5 regulate PME activity during disease. A) Schematic representation of the binding of Ruthenium Red to de-methylesterified pectin. **B)** Leaves of Arabidopsis WT and of *sbt* mutants were inoculated with *Botrytis* and Mock and PME activity were quantified at 24-hour post inoculation (hpi). The results represent the mean ± SD (n = 6). The different letters on the bars indicate datasets significantly different according to ANOVA followed by Tukey's test ($P < 0.05$).

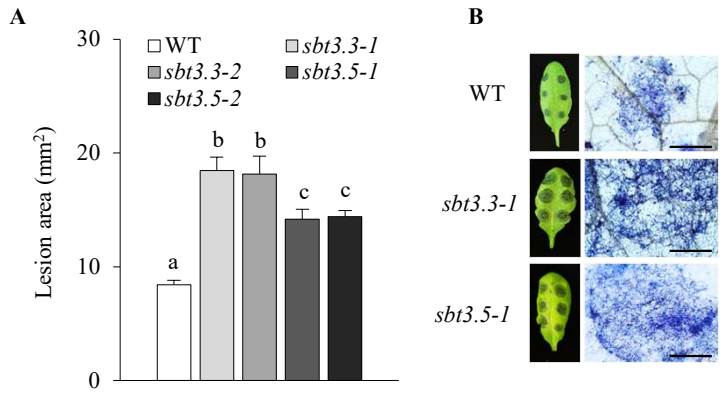

Figure 4. The lack of *SBT3.3 and SBT3.5* expression reduces *Arabidopsis* resistance to *Botrytis cinerea*. A) Quantification of lesion areas produced by the spreading of the fungus at 24 hours post infections. Data represent mean ± SE (n ≥14 lesions for each genotype). Different letters indicate statistically significant differences, according to ANOVA followed by Tukey's significance test ($P < 0.05$). **B)** Photographs showing lesion areas produced by *Botrytis* on leaves of Arabidopsis WT, *sbt3.3-1 and sbt3.5-1* mutants (left) and microphotographs showing *Botrytis* colonization revealed by trypan blue staining (right). Bars = 1mm.

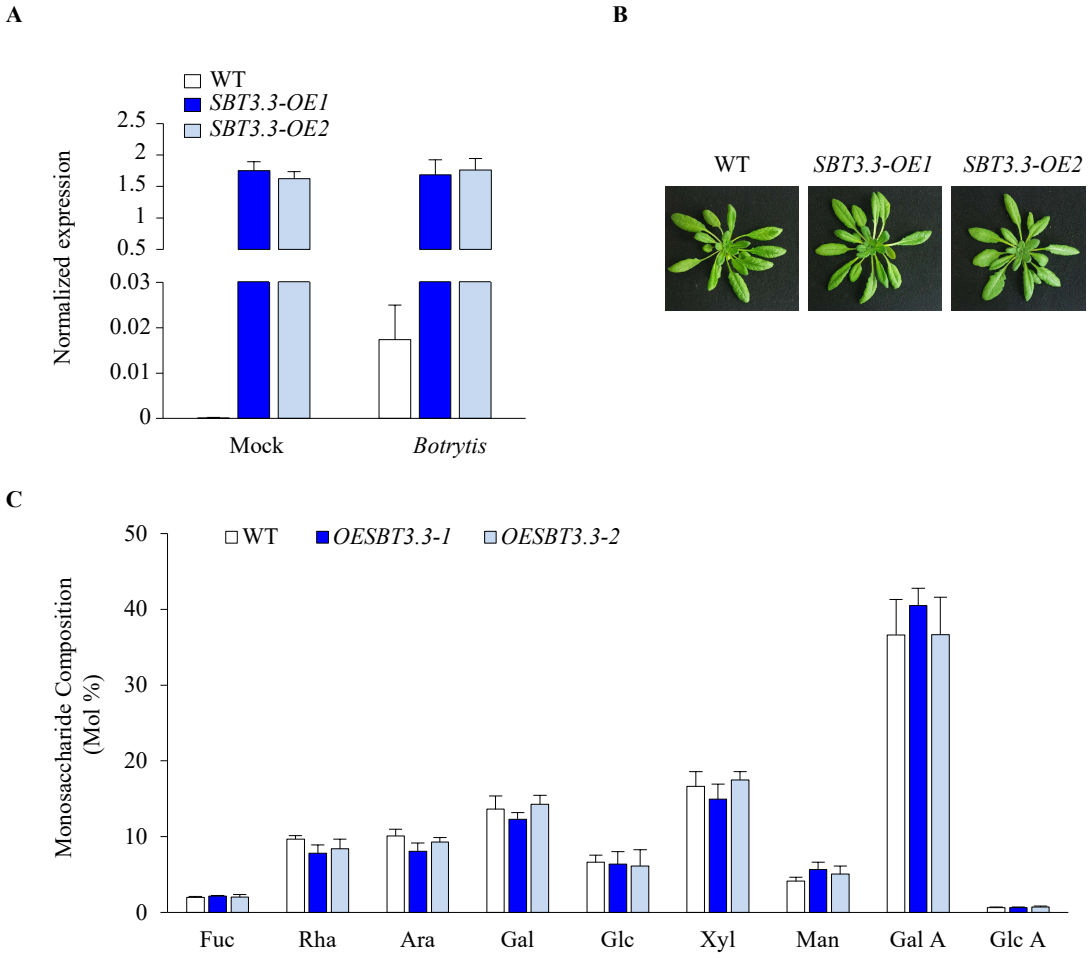

Figure 5. The *SBT3.3* overexpression in Arabidopsis does not alter rosette growth and cell wall composition. A) The expression of *SBT3.3* was analyzed in the *SBT3.3-OE1* and *SBT3.3-OE2* transgenic plants at 24-hour post inoculation with Mock and *B. cinerea* spores. The expression levels were normalized to *Ubiquitin5* expression. The experiments were repeated three times with similar results. **B)** Representative pictures illustrating the morphology of vegetative rosettes of *SBT3.3* overexpressing plants compared with WT plants. **C)** The molar percentages of Fucose (Fuc), Rhamnose (Rha), Arabinose (Ara), Galactose (Gal), Glucose (Glu), Xylose (Xyl), Mannose (Man), Galacturonic Acid (Gal A) and Glucuronic Acid (Glc A) were quantified. The results represent the mean ± SD ($n \geq 3$). Monosaccharide datasets are not significantly different according to analysis of variance (ANOVA) followed by Tukey's test ($P < 0.05$).

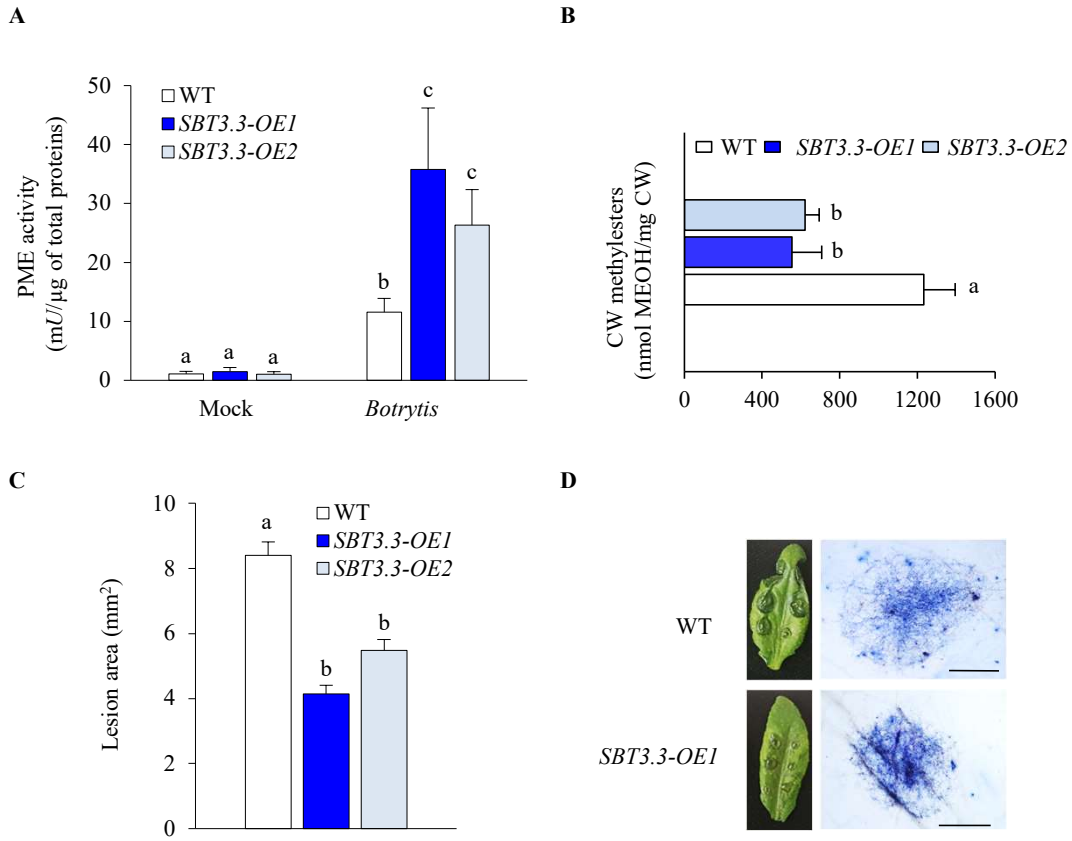

Figure 6. The *SBT3.3* overexpression overactivates PME activity restricting *Botrytis* infection. A) Leaves of Arabidopsis WT and of *SBT3.3-OE* plants were inoculated with *Botrytis* and Mock and PME activity were quantified at 24-hour post inoculation. The results represent the mean ± SD (n = 6). **B)** The amount of methylesters in the cell wall were quantified at 24-hour post inoculation. The results represent the mean ± SD (n = 6). **C)** Quantification of lesion areas produced by the spreading of the fungus at 24 hours post infections. Data represent mean **±** SE (n≥15 lesions for each genotype). **D)** Photographs showing lesion areas produced by *Botrytis* on leaves of WT and *SBT3.3-OE1* plants (left) and microphotographs showing *Botrytis* colonization revealed by trypan blue staining. Bars = 1mm. The different letters in A, B and C indicate datasets significantly different according to ANOVA followed by Tukey's test ($P < 0.05$).

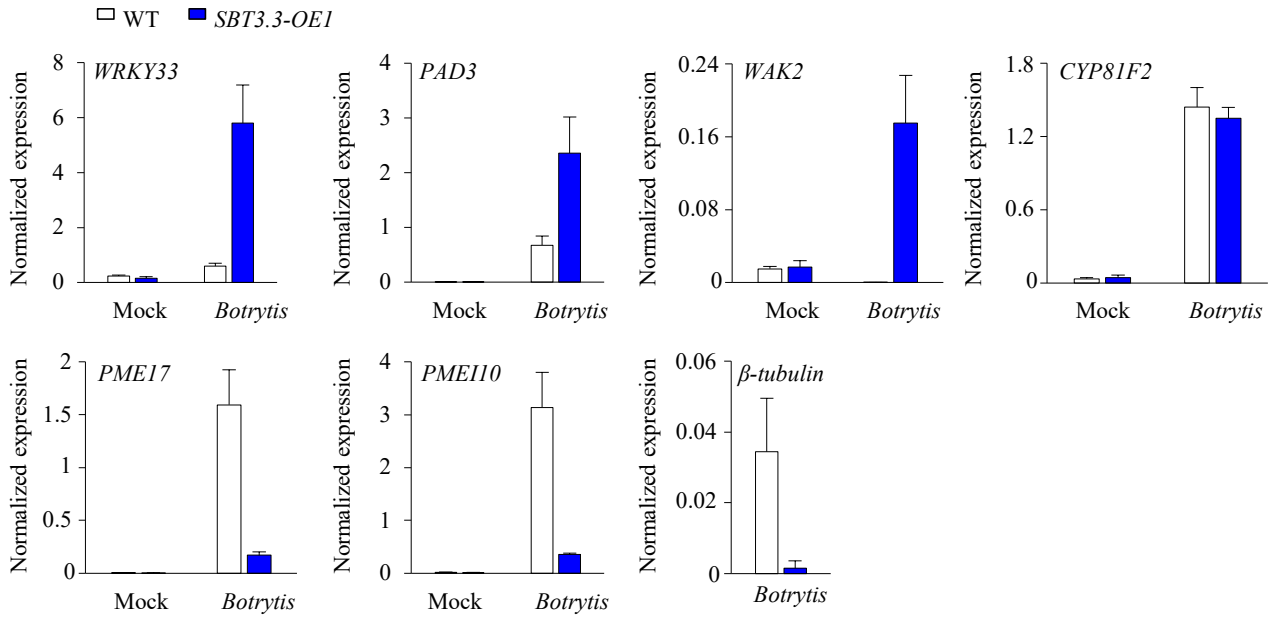

Figure 7. *SBT3.3* overexpression enhances immune responces. The induction of the expression of defence genes *WRKY33, PAD3, WAK2, CYP81F2, PME17, PMEI10* were compared between *SBT3.3-OE1* line and WT plants challenged with *Botrytis*. The mRNA expression was analysed at 24 hpi in *B. cinerea*- or mock-inoculated leaves by qPCR. *Botrytis β-tubulin* expression was also quantified. The expression levels were normalized to *Ubiquitin5* expression. The experiments were repeated three times with similar results.

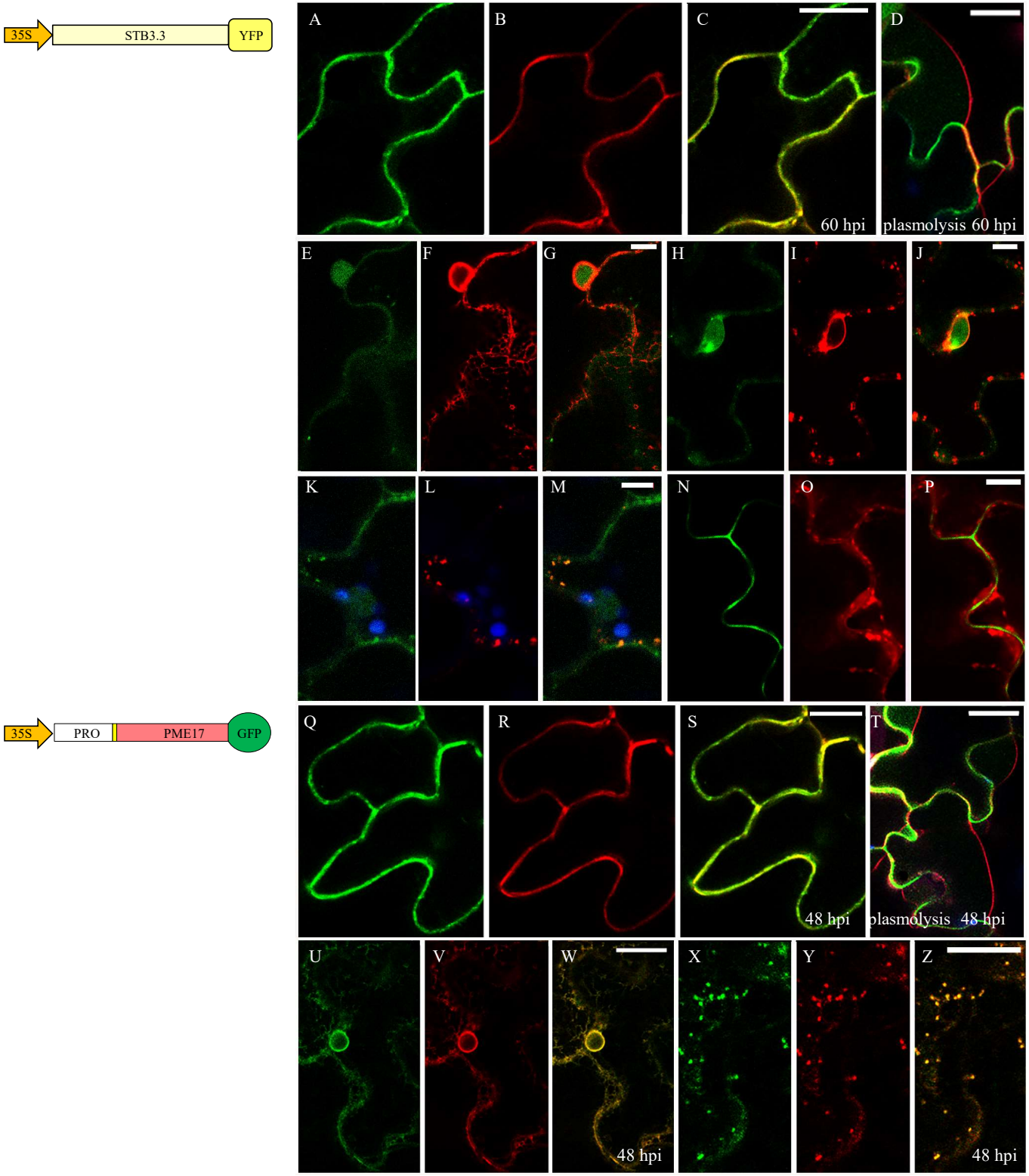

Figure 8. SBT3.3 and Pro-PME17 are delivered in the apoplast through different protein secretion pathways. Confocal microscopy images of epidermal cells of *Nicotiana tabacum* adult leaves showing the coexpression of SBT3.3-YFP (**A-P**) or Pro-PME17-GFP (**Q-Z**) with different markers of subcellular compartments (**B-C-, R-S:** XTH11-RFP, cell wall; **F-G, V-W** RFP-HDEL, endoplasmic reticulum; **I-J, Y-Z:** ST52-mCherry, Golgi stacks) at the indicated hours post infiltration (hpi). Plasmolyzed cells (1 M NaCl) expressing SBT3.3-YFP or Pro-PME17-GFP and the plasma membrane marker pm-rk show the green fluorescent cell wall and the retracted red fluorescent plasma membrane (**D, T**). Chlorophyll autofluorescence within the chloroplasts is depicted in blue. Scale bars = 20 µm (**A-C, Q-S**), 10 µm (**E-P**, **U-Z**), and 5 µm (**D, T**).

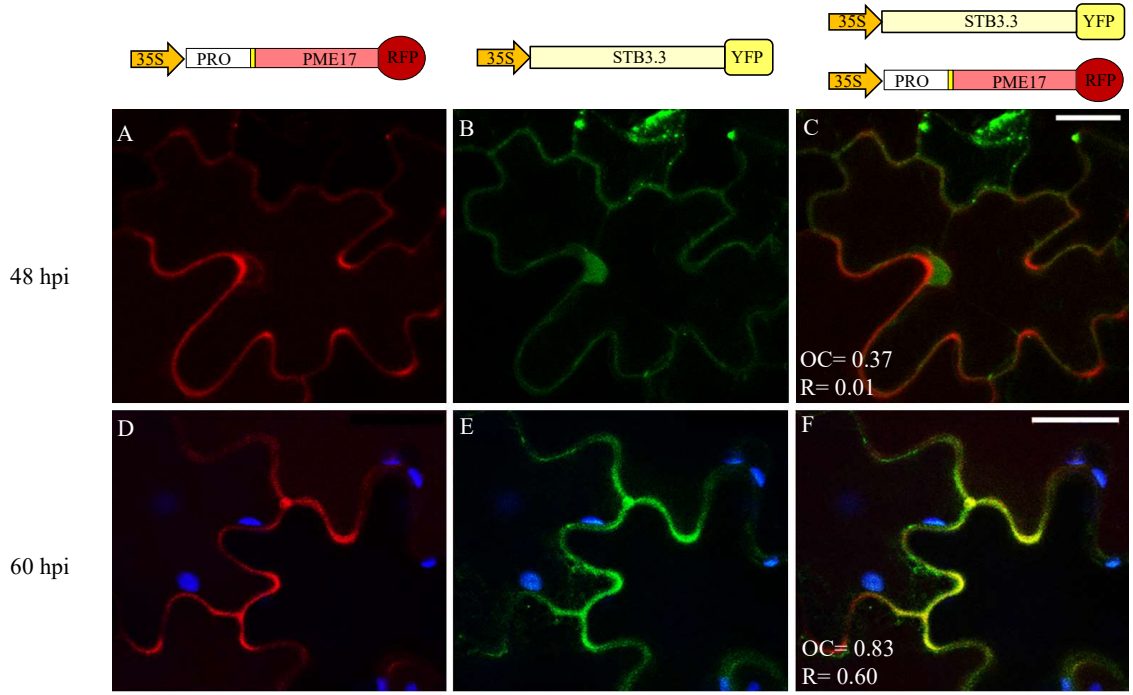

Figure 9. Pro-PME17 and SBT3.3 colocalize in the cell wall and their colocalization is favoured over time. Confocal microscopy images of epidermal cells of tobacco adult leaves co-expressing Pro-PME17-RFP (**A** and **D**) and SBT3.3-YFP (**B** and **E**) at the indicated hours post infiltration (hpi). Merged images showing the co-localization of SBT3.3-YFP and Pro-PME17-RFP in the cell wall (**C** and **F**). Overlap coefficient (OC, after Manders) and R (Pearson's correlation coefficient) values are reported in each merged image. Chlorophyll autofluorescence within the chloroplasts is depicted in blue. Scale bars = 20 µm.